Characterization of Amyloid Fibril Formation in a Microfluidic Chip

Tuuli Hakala

School of Electrical Engineering

Thesis submitted for examination for the degree of Master of Science in Technology.

Espoo April 18, 2016

Thesis supervisor and advisor:

Prof. Paavo Kinnunen

Aalto University
School of Electrical
Engineering

AALTO UNIVERSITY
SCHOOL OF ELECTRICAL ENGINEERING

ABSTRACT OF THE
MASTER'S THESIS

Author: Tuuli Hakala

Title: Characterization of Amyloid Fibril Formation in a Microfluidic Chip

Date: April 18, 2016 Language: English Number of pages: 7+66

Department of Neuroscience and Biomedical Engineering

Professorship: Molecular Biophysics

Supervisor and advisor: Prof. Paavo Kinnunen

Amyloid fibrils are protein aggregates known for their unique β-sheet rich structure and involvement in multiple diseases. Hence, these self-assembling aggregates have aroused the interest of scientist from multiple different fields, and new strategies to study and observe amyloid formation are pursued after.

This thesis introduces two novel approaches for characterization of amyloid formation. A microfluidic chip that allows a direct observation with an inverted microscope and impedance measurements with surface electrodes was designed. In the first approach, a continuous network of highly fluorescent peptide aggregates were formed. This was possible by utilizing a laminar flow in a micro channel and concentration gradients of peptides and lipids between adjacent streams. An intrinsic fluorescence with a wide spectrum was observed with all peptides. Even higher emission was detected in the presence of pyrene-labelled lipids, suggesting strong interaction between adjacent pyrene moieties. The second method involved impedance measurements of a supported lipid bilayer (SLB). In addition, the effect of amyloidogenic peptides on the SLB conductivity was determined. Hence, the SLB was used as a sensor for lipid-amyloid interaction and assembly. The introduction of peptides into the bilayer showed decrease of conductivity indicating reorganization of phospholipids in the SLB.

The results provided novel information from the amyloid-lipid interaction and could serve as possible characterization tools for amyloid research.

Keywords: amyloid formation, microfluidics, supported lipid bilayer, intrinsic fluorescence, and impedance

AALTO-YLIOPISTO
SÄHKÖTEKNIIKAN KORKEAKOULU

DIPLOMITYÖN
TIIVISTELMÄ

Tekijä: Tuuli Hakala

Työn nimi: Amyloidien muodostumisen karaterisointi mikrofluidistisessa kammiossa

Päivämäärä: April 18, 2016 Kieli: Englanti Sivumäärä: 7+66

Neurotieteen ja lääketieteellisen tekniikan laitos

Professuuri: Molekulaarinen biofysiikka

Työn valvoja ja ohjaaja: Prof. Paavo Kinnunen

Amyloidit ovat proteiiniaggregaatteja, jotka tunnetaan niiden ainutlaatuisesta β-laskos rikkaasta rakenteestaan, sekä osallisuudesta moniin sairauksiin. Tästä johtuen tutkijoiden kiinnostus on herännyt ja uusia parempia metodeja amyloiditutkimukseen pyritään kehittämään.

Tämä työ esittelee kaksi uutta menetelmää amyloidien karakterisointiin. Tätä varten suunniteltiin mikrofluidistinen siru, joka mahdollisti suoran visuaalisen havainnoinnin mikroskoopilla ja pintaelektrodeilla suoritettavat impedanssimittaukset. Ensimmäisessä menetelmässä luotiin yhtenäinen verkosto vahvasti fluoresoivia peptidi aggregaatteja. Tämä oli mahdollista hyödyntämällä mikrokanavassa olevaa laminaarivirtausta ja vierekkäisten peptidi- ja lipidivirtojen konsentraatiogradienttia. Kaikilla käytetyillä peptideillä havaittiin sisäsyntyistä fluoresenssia laajalla spektrillä. Korkein emissio saatiin aikaiseksi, kun osa lipideistä oli leimattu pyreenillä. Tämä viittaa vahvaan vuorovaikutukseen pyreeniosien välillä. Toisessa menetelmässä käytetiin impedanssispektroskopiaa tuetun lipidikaksoiskalvon (SLB) johtuvuuden karakterisointiin. Lisäksi amyloideja muodostavien peptidien vaikutus SLBn johtuvuuteen määritettiin. Näinollen SLBtä käytettiin sensorina lipidi–amyloidi vuorovaikutukselle ja amyloidien muodostumiselle. Peptidien lisääminen lipidikaksoiskalvolle laski SLBn johtuvuutta, mikä viittaisi fosfolipidien uudelleen järjestäytymiseen kalvossa.

Nämä tulokset osoittavat, että käytetyt menetelmät tuottivat uutta tietoa amyloidien ja lipidien välisestä vuorovaikutuksesta. Lisäksi menetelmät voisivat toimia mahdollisina karakterisointi välineinä amyloiditutkimuksessa.

Avainsanat: amyloidien muodostuminen, mikrofluidistiikka, tuettu lipidikaksoiskalvo, sisäsyntyinen fluoresenssi ja impedanssi

Preface

The experimental work for this thesis was done in Aalto University, The Department of Neuroscience and Biomedical Engineering in Professor Paavo Kinnunen's lab Helsinki Biophysics and Biomembrane Group. The greatest gratitude goes to prof. Paavo Kinnunen from this opportunity and guidance through these years. In addition, I want to thank all other group members from their support and stimulating discussions. Especially, thank you Sakari for sharing your expertise in impedance spectroscopy and electrical measurements.

Great gratitude also to my parents and brother, who have encouraged me in my studies and choices through the years. Last, but not least, thank you Aleksi for you unconditional support.

Otaniemi, April 18, 2016

Tuuli A. Hakala

Contents

Symbols and Abbreviations

Symbols

Amyloid formation:

A	The final value in plateau
y_0	Base line
r_{max}	Maximum growth rate
τ_{lag}	Lag time
τ_{50}	Time for aggregate mass to reach 50 % of its final value

Phospholipids:

a_0	The effective area per head group
p	Packing parameter
v	Volume for the hydrophobic portion of the lipid
l	The length of the acyl chains

Microfluidic environment:

a	Acceleration due to the gravity
Bo	Bond number
D	Diffusivity
η	Viscosity of a fluid
γ	Surface tension
k_B	Boltzmann constant
L	The characteristic length of a microfluidic channel
Pe	Péclet number
Re	Reynolds number
ρ	Density
v	Velocity of a flow

Sample preparation:

A_{342nm}	Absorbance (Wavelength 342 nm)
C	Concentration
ε	Extrinsic constant of a fluorophore
x	Dilution factor

Electronics:

C	Conductance
I	Current
L	Inductance
R	Resistance
U	Voltage drop
V	Voltage
X	Reactance
Z	Impedance

Abbreviations

Aβ	Amyloid beta peptide
ACN	Acetonitrile
AFM	Atomic-force microscopy
AFU	Adaptive focused ultrasound
CMC	Critical micelle concentration
CPB	Cycles per burst
DC	Duty cycle
DSPamp	DSP SR830 Lock-in amplifier
EDTA	Ethylenediaminetetraacetic acid
EM	Electron microscopy
FRAP	Fluorescence recovery after photobleaching
FTIR	Fourier transform infrared spectroscopy
HDMS	Hexamethyldisilazane
HEPES	4-(2-hydroxyethyl)-1- piperazineethanesulfonic acid
KIGAKI	$[KIGAKI]_3$-NH_2
LUV	Large unilamellar vesicles
Mf	Microfluidics
MES	2-(N-morpholino)-ethanesulfonic acid
MLV	Multilamellar vesicles
ox-pl	Oxidized phospholipid derivative
PA	Phosphatic acid
PC	Phosphatidylcholine
PG	Phosphatidylglysesrol
PE	Phosphatidylethanolamine
PI	phosphatidylinositol
PS	phosphatidylserine
PDMS	Polydimethylsiloxane
$PolyK_{10}$	Poly-lysine with 10 lysine residues
POPC	1-palmitoyl-2-oleoyl-sn-glycero-3-phosphocholine
POPG	1-palmitoyl-2-oleoyl-sn-glycero-3-phospho-rac-glycero
PPDPC	1-palmitoyl-2[6-(pyren-1-yl)]decanoyl-sn-glycero-3-phosphocholine
PPDPG	1-palmitoyl-2-[(6-pyren-1-yl)]decanoyl-sn-glycero-3-phospho-rac-glycerol
RMS	Root mean square
SLB	Supported lipid bilayer
SUV	Small unilamellar vesicles
TempB	Temporin B
ThS	Thioflavin S
ThT	Thioflavin T
4T sensing	Four-terminal sensing

1 Introduction

Amyloids are insoluble protein structures with a β-sheet rich content. The β-sheets are assembled parallel to each other to form highly organized fibrillar structures. These so called amyloid plaques are connected to multiple different diseases such as Alzheimer dieses with Amyloid Beta peptide plaques, Parkinson's disease with α-synuclein aggregates and type II diabetes with islet amyloid peptide (IAPP) aggregates. [1]

Although peptides can form multiple different conformations and aggregates, amyloid fibrils are considered to be unique due to their highly ordered and stable 'misfolded' structure. The kinetics of the protein folding can be explained through energy landscapes, where various states of the protein folding may exist. Amyloid fibrils are considered to be at the bottom of the energy landscape, meaning that it is the most stable form of aggregation. [1]

Previous experiments have demonstrated multiple different strategies to effect the amyloid formation *in vitro*. In addition to experimental conditions such as pH, salt ions, temperature, stirring etc., it has been shown that the acidic [2–4] and oxidized lipids [5] can promote the amyloid formation by changing the local concentration, conformation and stability of the peptides. [5, 6]

Amyloid fibres are good example of molecular self-assembly. Although they are well known for their role in diseases, amyloid fibrils are attracting increasing interest for molecular electronics applications [7]. Hence, due to their size and wire–like structure amyloid are attractive option to be used as nano-wires in future electronic devises. [8] However, pure amyloid-like fibrils have not manifested great promise as a charge carriers [7]. Instead they are suggested to be used as a scaffolds for other conductors [8]. Despite the previous unsuccessful studies, L. del Mercato et al (PNAS, 2007) where able to measure nano ampere currents flowing through amyloid like nanofibers [7]. In addition, they observed intrinsic fluorescence in amyloid fibres suggesting the presence of delocalized electrons that could serve as charge carriers. [7, 9–11]

Most of the amyloid studies are conducted in bulk, however there are increasing number of studies demonstrating microfluidic solutions to investigate the amyloid formation [12–17]. Microfluidic chamber with a sub millimetre length scale has evolved to be a proficient method also in various other biological studies such as drug discovery [18] and single cell analysis [19]. In addition to small length scales, the reduced sample volume, easy fabrication of tailored experiment system, and possibility to create automated high throughput systems attract scientist to experiment with microfluidics. Furthermore, the plaque deposition in pathological condition is associated with surfaces, thus amyloid deposit studies with a solid surface is regarded to be more relevant than experiments in a bulk solution [20]. Supported lipid bilayers (SLB) have been used as cell surface models in amyloid studies [21, 22], but also the microchannel surface can act as a template for amyloid formation [12].

Fluorescence is one of the most used methods in amyloid research. The amyloid specific fluorescent dyes are used to observe and follow the kinetics of amyloid formation. However, these can produce false results, hence electron microscopic methods are used to confirm the characteristic fibrillar nano structure of amyloids. In addition to false results, these dyes can induce the amyloid formation affecting the result. Because of these problems, new better strategies for amyloid studies are relevant to be investigated. [23]

The aim of this thesis was to find novel characterization approaches for the formation of amyloid fibres in a microfluidic chip. The chosen methods were: fluorescent microscopy and impedance measurements. For the former, a method to form continuous network of aggregates to produce detectable intrinsic fluorescence was established. In the latter, a microfluidic chamber with surface electrodes were fabricated to perform impedance spectroscopy experiments. The hypothesis was, that the amyloid fibril formation would change the organization of supported lipid bilayer deposited on top of the electrodes, thus changing the impedance of the system. In other words, the SLB was expected to work as a sensor for amyloid formation.

2 Theoretical Background

This section describes the theoretical background for the topics of this Master's Thesis. First, the terms amyloid and phospholipid are introduced. This is followed by the discussion of the influence of phospholipids to protein structure. Additionally a short theory of fluorescence and self-assembled monolayers is covered. Lastly, the concept of microfluidics and characteristics of the microfluidic environment are discussed followed by introduction to previous research of amyloids in a microfluidic systems.

2.1 Amyloids

Proteins are formed from one or several polypeptides that consist of amino acids linked to each other by peptide bonds. There is vast multitude of conformational states available for these polypeptide chains. This can be schematically depicted with an energy landscape surface (Fig. 1). The simple folding funnels, represented by light grey area, describes the conformational search of a single polypeptide chain with a random coil structure to a functional monomer. The dark grey represents intermolecular protein association that dramatically increases ruggedness of the landscape. The landscape illustrates the complexity of a protein folding and variation of aggregation energy. Thus, having multiple different conformational states and variety of available pathways to each polypeptide chain while it travels around the landscape. [24, 25]

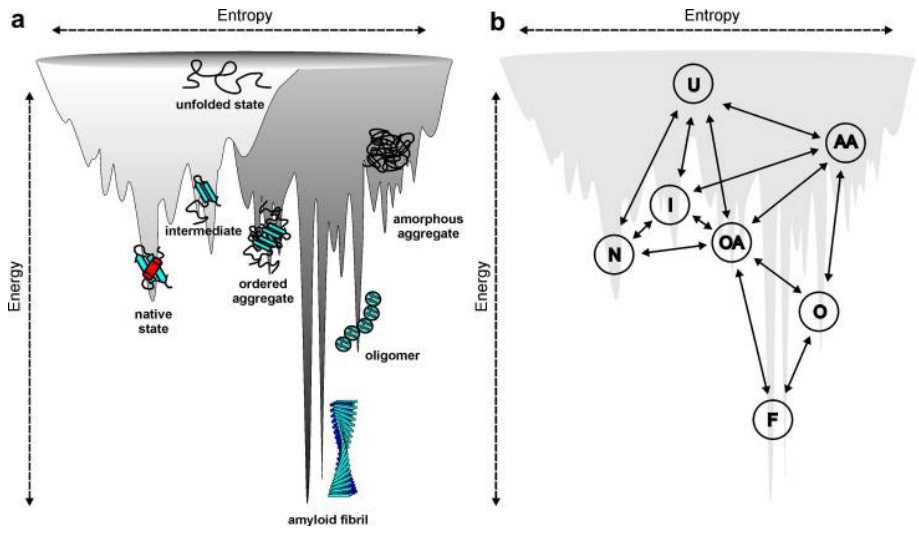

Figure 1: a) Illustration of energy landscape for protein folding and b) examples of different pathways to amyloid fibril formation. Adapted from Ref: [25]

Some proteins tend to adopt a certain sub-molecular conformation that has a sharper and deeper energy minimum than native monomeric proteins, called an amyloid conformation. [26] In this conformation proteins form well ordered fibrillar aggregates,

amyloid fibres, which have been identified to be involved in multiple different diseases. Hence, they have been under intense research.

Amyloids possess cross-β structure in which the hydrogen bonding direction runs parallel to the fiber axis. All the β strands are perpendicular, resembling the rungs of a ladder. This highly ordered hydrogen network in considered to be responsible from the rigidity of amyloids. [27]

Due to their insoluble and heterogeneous nature, the use of conventional structure characterization methods is difficult [25]. However, experiments with electron (EM) [28] and atomic force microscopy (AFM) [29] have suggested, that amyloid fibrils are formed from individual subunits named "protofilaments". The number of protofilaments may vary in number and twist around one another in mature amyloid fibril (Fig. 2 a). [28].

2.1.1 Theory and Study Methods of Amyloid Formation

The formation of amyloid fibrils is not fully understood, but it has been suggested that the fibrils form by nucleation dependent mechanism. Typically the nucleation growth mechanism shows a lag phase (τ_{lag}) followed by a rapid extension reaction called a growth phase, and finally settling to a certain value in a plateau phase. This is called a sigmoidal behaviour. (Fig. 2 b). The time for aggregate mass to reach 50% of its final value (τ_{50}) is also the time in which the maximum growth rate (r_{max}) occurs. By finding the points were tangent drawn to r_{max} meet time axis, and the final value of the fibril mass the lag, growth and plateau phases can be differentiated. [30] A mathematical approach to this is to use a sigmoidal function to fit the growth data and determine the wanted parameters. The function used is:

$$y = y_0 + \frac{A}{1 + exp(-k(t - \tau_{50}))}, \tag{1}$$

where y_0 is the base line, A the amplitude and t is time. The lag time is defined as $\tau_{lag} = \tau_{50} - 1/2k$ [31].

During the lag phase multiple parallel processes co-exist. In the beginning of the process millions of primary nucleus form, and lag phase exhibits the time that these nucleus requires to grow and proliferate. Fibrils grown from primary nucleus may present a catalytic surface for the formation of new aggregates in a process called: secondary nucleation. Alternatively, the fibrils might break in a fragmentation, hence providing new ends for elongation. [31]

The duration of the lag phase can be as long as days, thus multiple strategies for precipitation or removal of lag phase have been employed. For example, pre-formed seeds such as nucleation or prefibrillar solutions can be applied [32]. In addition, experimental conditions including high pH, salt ions, elevated temperature, and

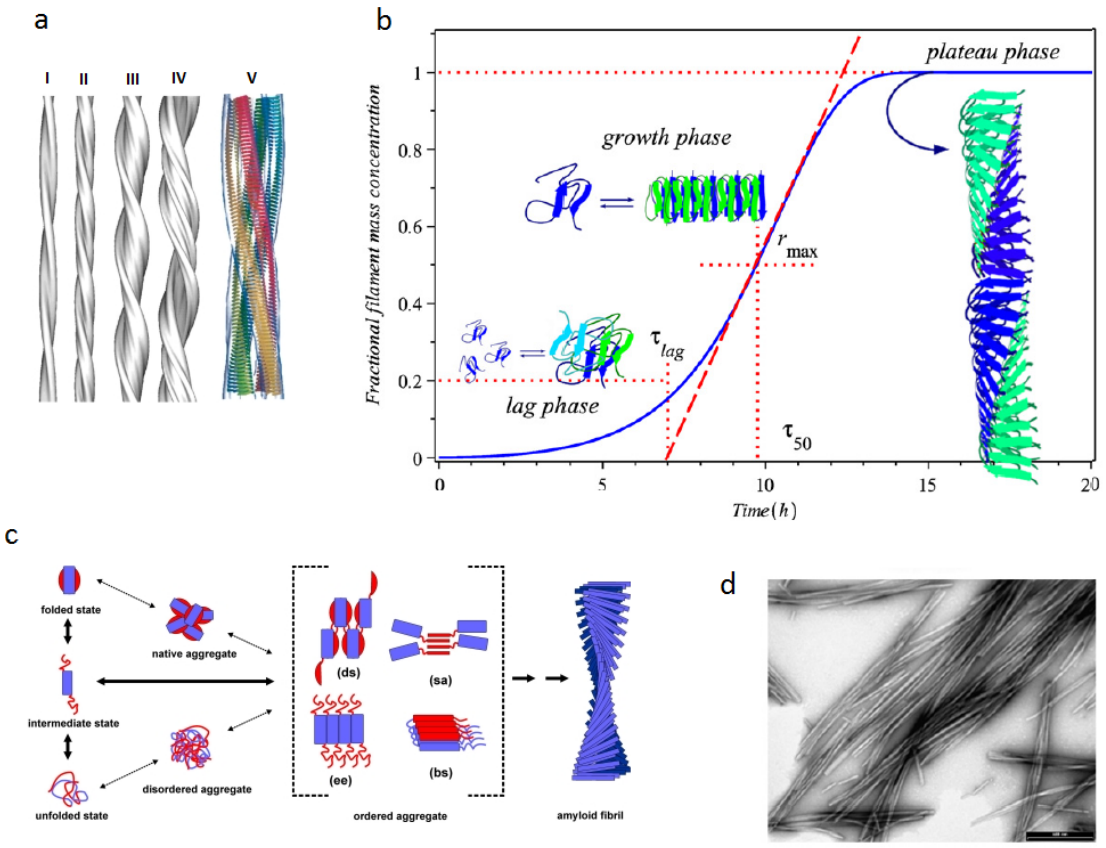

Figure 2: a) 3D maps obtained from electron microscopy studies for insulin fibril structures. The mature fibrils can consist from either two (I), four (II) or six (III and IV) protofilaments. V) A proposed β-sheet structure for insulin with four protofilaments. b) A sigmoidal growth profile of fibril mass formation and typical parameters. c) Proposed method for amyloid formation. For many peptides the formation starts from partially unfolded native structure that proceeds to intermediate folded states. These can form ordered aggregates in multiple ways such as: domain swapping (ds), strand association (sa), edge-edge-association (ee) or β-strand stacking (bs). By self-association and possibly further conformational changes the amyloid fibrils are formed. d) A transmission electron micrograph of TTR105–115 fibrils (scale bar 500 nm). Adapted from Ref: [25, 30]

stirring can be used to affect the lag phase in in vitro studies [31, 33, 34]. For many peptides the amyloid formation begins from a partially unfolded native structure. Thus, to achieve this, high pH or elevated temperature are commonly used in amyloid studies. It is proposed that these unfolded structures can take multiple pathways to reach a mature amyloid fibril state (Fig. 2 c) [25].

Multiple different aspects of amyloid fibril formation can be characterized *in vitro*, including the identification of the amyloid structure and the process of fibril formation. There are multiple methods for identifying amyloid fibrils. Firstly, the fibrillar nano

structure can be characterized using electron microscope (EM) techniques such as atomic-force microscope (AFM) and transmission electron microscope (TEM) (Fig. 2 d). Secondly, the β- sheet morphology can be confirmed using Fourier transform infrared spectroscopy (FTIR) or x-ray crystallography. Thirdly, there are multiple different amyloid specific fluorescent dyes that can be employed for amyloid detection or kinetics studies. The most commonly used dyes are: Congo Red, Thioflavin S and T (ThS and ThT). It is argued that at least two of these techniques should be used to avoid interpretation errors (false positive and negative) in amyloid experiments. [23] In addition to these traditional methods, new and better ways to detect and study amyloids have been suggested and are under research. [11]

Recently it was observed that upon excitation with UV-light, amyloid fibrils emit violet blue radiation. [9] It is proposed that this intrinsic fluorescence can originate from the hydrogen bond rich cross-β structure. Thus, the hydrogen bonds formed by C=O and N–H atom groups between peptides can potentially cause delocalization of some electrons in the orbitals of peptide bonds. These electrons have the potential to show such long-wavelength low-energy transitions observed. Similar observations and more analysis from the intrinsic fluorescence have been done also with other peptides and excitation wavelengths [7, 10, 11]. Further, it is suggested that this fluorescence can be used to perform a label-free assays to monitor fibril growth. [11]

Amyloids are not the only type of proteins that possess fluorescent properties. A protein with a beta barrel structure, called green fluorescent protein is extensively used for its fluorescent properties. [35]

2.1.2 Conductivity Measurements of Amyloids

The study of the amyloid formation has applications beyond the relationship to human disease. The studies has provided insights into normal protein folding and the evolution of protein folding. In addition, the highly arranged structure of amyloids has sparked considerable interest in the use of amyloid fibrils for nanotechnology and other applications in material science. [23]

Nanowires are potential building blocks for future electronic devices. Nonetheless, the difficulty is the construction of such small structures. Self-assembling biomolecules might be the solution to this problem, due to their natural size. Amyloid fibres are attractive option because of their wire–like structure and great strength. However, the intrinsic properties of biomolecules are generally unsuitable for conducting electrical currents; therefore they are usually combined with an inorganic compound that acts as a conductor. [8]

L. Del Mercato and co-workers have shown conductivity of amyloids in their study of charge transport and intrinsic fluorescence in Poly(ValGlyGlyLeuGly) amyloid-like fibrils. They deposited 10 μl of 1.0 mg/ml fibril suspension in ultrapure water onto electrode structures fabricated on SiO_2 substrate. The water was evaporated by letting the sample be in ambient environment overnight.

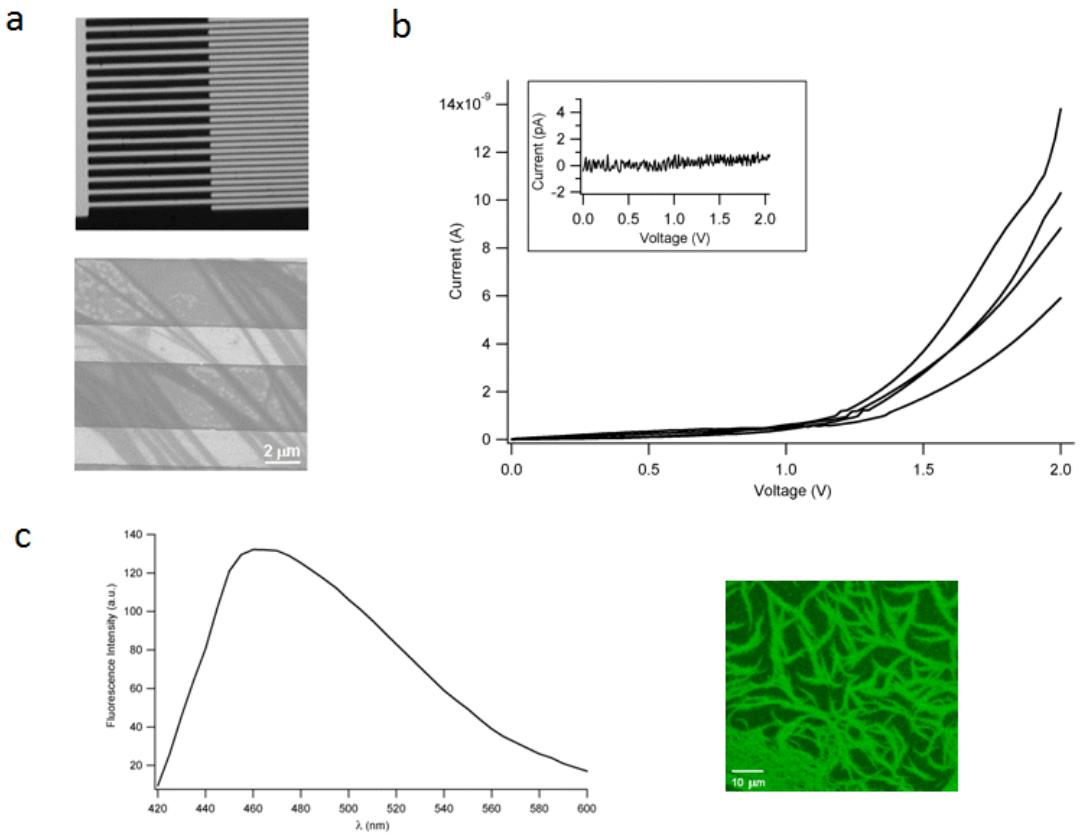

Figure 3: a) SEM image of the interdigitated electrodes used for electron transport experiments and representative SEM micrograph of the electrodes after fibrils deposition. b) Current-voltage characteristics of nanofibrils. c) Intrinsic fluorescence spectrum of poly(ValGlyGlyLeuGly) amyloids and confocal microscopy image of the fibrils (excitation in both wavelength, 405 nm) Adapted from Ref: [7].

They recorded several nano-Ampere (nA) currents from amyloid bridges, corresponding to impedances in hundred MΩ range. The current value was observed to be dependent on the number of amyloid fibrils bridging the electrodes and environmental conditions. By chancing the humidity they found out that water molecules have a primary role the in charge transport of amyloid fibrils. [7].

In addition, fluorescence intensity spectrum was recorded from the fibrils (Fig. 3 c), showing characteristic intrinsic fluorescence spectrum of amyloids. Hence, emission spectrum had a broad peak centring at 460 nm, when exited with 405 nm light. L. Del Mercato *et.al* demonstrated that this fluorescence was significantly decreased in vacuum, suggesting that hydrogen bonds between water molecules could play a role in the fluorescence emission of the fibrils.

Although the recorded conductivities by L. Del Mercato *et.al* are not even close to typical metal wire levels, it shows that amyloids could be potentially used as a charge carriers.

2.2 Phospholipids in Biological Membranes

Lipids and proteins are known to co-exist in biological membranes and the interaction between these groups of molecules serves essential functionalities to a living cell. Hence, a malfunction or a change in these molecular systems can be responsible for diseases. For example the role of lipids in amyloid formation has been extensively studied. Before we can understand the nature of these interactions, the structure of phospholipids and lipid-membranes must be discussed.

2.2.1 Introduction to Phospholipids and Lipid membranes

Phospholipids are a major component of all cellular membranes. They are built from a phosphate containing polar head and one or two long apolar alkyl chains (Fig. 4). The hydrophilic head contain a negative phosphate with a specific head group and glycerol. Long alkyl chains are connected to the glycerol part of polar head by ester or ether bonds. Due to the hydrophobicity of these hydrocarbon chains, individual lipids are poorly soluble in water. However, their amphiphilicity promotes a spontaneous assembly of supramolecular aggregates, such as micelles, liposomes and bilayers. [36]

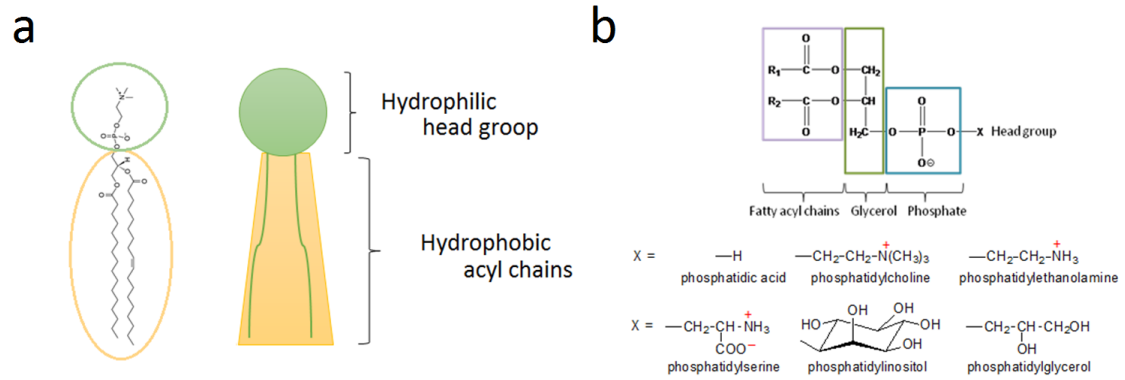

Figure 4: a) POPC as an example of a phospholipid and simplified schematic figure of a phospholipid. The hydrophobic regions are surrounded with yellow colour and the hydrophilic headgroup with green circle. b) Structure and major classes of phospholipids: phosphatic acid(PA), phosphatidylcholine (PC), phosphatidylethanolamine (PE), phosphatidylserine (PS), phosphatidylinositol (PI) and phosphatidylglysesrol (PG). Adapted from Ref: [37].

It is assumed that the free energy of an amphiphilic molecule in aqueous solution, such as phospholipid, is the result of three terms: hydrophobic contribution, surface term, and packing term. The hydrophobic contribution is due to separation of acyl chains from the water. Consequently, the lipid headgroups have a tendency to crowd together to minimize the un-favourable alkyl chain contacts with water, creating the surface term. However, this crowding is confined by electrostatic repulsion of

negative head groups and steric hindrance. The packing term excludes the water and headgroups from the hydrophobic interior, thus setting a limit to geometrical forms that the lipid aggregate can take. The surface and packing terms differ for each aggregate geometry. For different conditions the aggregate structure giving the minimal free energy vary. In other words, just by changing ambient conditions in aqueous solution, same phospholipid can adopt different supramolecular aggregate structures. [38]

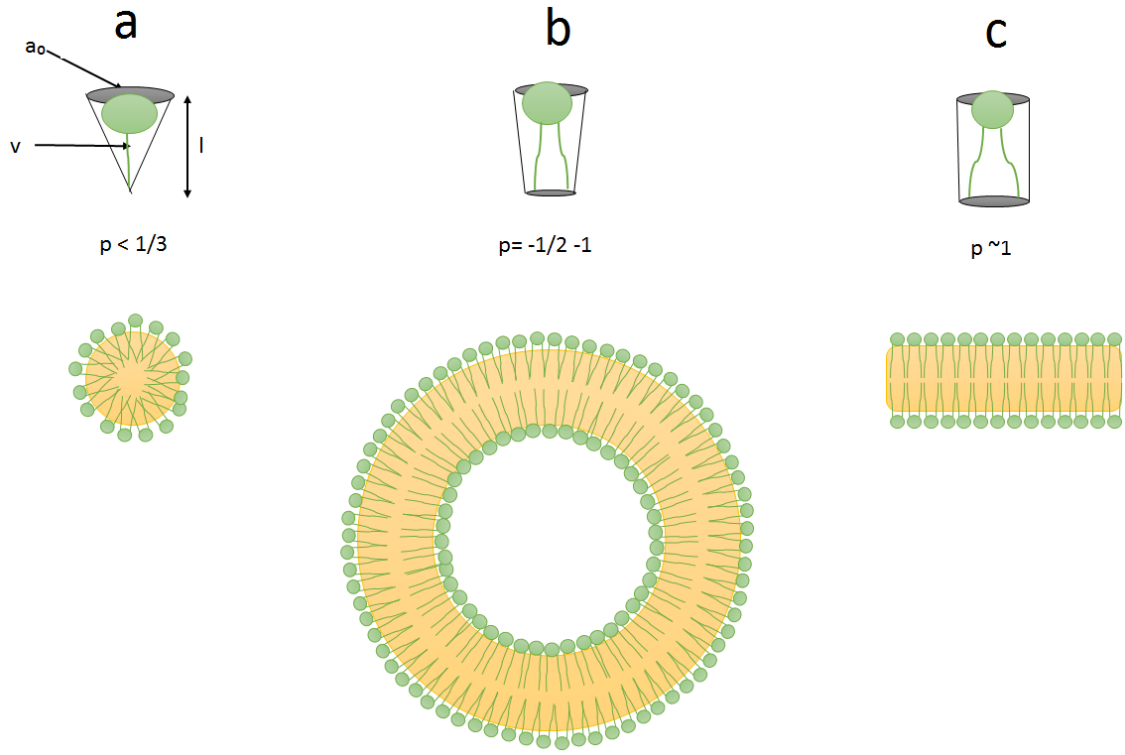

Figure 5: Schematic illustration from a) micelle, b) liposome and c) bilayer and the relevant packing shapes and parameters. The hydrophobic environment created by the long acyl chains is highlighted by yellow colour.

In order to predict the lipid shape-structure–relationship between monomeric lipids and their aggregates, a theoretical model was created [39]. The model defines a so called packing parameter (also called a surfactant parameter) for each lipid. This packing parameter can be represented by equation:

$$p = \frac{V}{la_0}, \tag{2}$$

where v stands for volume of the hydrophobic portion of the phospholipid, l is the length of the acyl chains and a_0 is the effective area per head group. The packing parameter can be used to find a representative packing shape for each lipid molecule. Similarly, the packing shape determinates the form of the supramolecular aggregate. Different packing parameter and corresponding shapes and supramolecular assemblies

are depicted in Figure 5. Single-chained lipids with a large head group have p value under $1/3$ and are represented with a cone packing shape (Fig. 5 a). Thus, these lipids form spherical micelles. For the lipids with smaller head group, the packing parameter is increased and the packing shape resembles a truncated cone. However, if the lipid has one acyl chain it has a p value between $1/3$ and $1/2$, and it forms cylindrical micelles. The double-chained lipids with a large head group, such as PC, PS, PC and PA lipids, have higher p values (Fig. 5 b). This makes them to adopt flexible bilayer structures such as liposomes. If the head group of the lipid is small enough the packing parameter is close to 1 (Fig. 5 c). These lipids do not possess the tendency to form curved structures, so they adopt flat bilayer surfaces. There are also other lipid aggregate structures with different packing parameter values, but they are not relevant to this thesis. [36, 38]

Lipid bilayer is extremely soft and lipids in it are constantly moving and undergoing a range of different dynamical processes. These processes include: conformational changes, rotation around the molecular axis of the lipid, lateral diffusion, protrusion out of the bilayer and flip-flop between the adjacent monolayers. The conformational changes takes only few pico seconds. Nano seconds are needed to the lipid to rotate around its axis. During this time the lipid has also travelled distance of its own size. Contrary to these quick movements the flip-flop of lipid can take anything from hours to days. [36]

The free diffusion of lipid molecule can be obstructed by so called phase separation of the membrane. A single component phase separation is caused by the possible existence of lipid in multiple phase states. For biomembranes mostly lamellar states are relevant, and these include: liquid-disordered, solid-ordered and liquid-ordered. Depending on the lipid composition of the membrane eater one or multiple phases can co-exist. [40] Multi-component lipid bilayers can imply solid and liquid phases, as well as solid–solid, solid–liquid, as liquid–liquid phase separation [41]. The occurrence of differentiated regions caused be the phase separation are called domains [42].

The saturation of the fatty acid side chains effects the membrane fluidity. The chains can be either saturated or unsaturated. In saturated side chains, all the carbon-carbon bonds are single, but in unsaturated side chains, one or more pairs of adjacent carbon atoms are linked by double bonds. Phospholipid layers consisting solely of saturated lipids are relatively rigid due to ordered aligned crystalline array structure. However, the double bonds in unsaturated fatty acids prompt bends in alkyl chains. Hence, packing of neighbouring molecules in phospholipid bilayers containing unsaturated lipids are less ordered, thus more fluid. [43, p. 77]

Phospholipid bilayers that are supported by substrates are robust and stable models of biological membranes. These so called supported lipid bilayers (SLBs) need a substrate that is hydrophilic, smooth, and clean. Good substrates for the SLB formation are fused silica (quartz), borosilicate glass, mica and oxidized silicon. One of the easiest and most versatile way to form the SLB is by adsorption and fusion of small unilamellar lipid vesicles (SUV) from an aqueous suspension to the substrate surface trapping a 10–20 å water layer between the substrate and bilayer. The exact

mechanism of the SLB formation is not fully understood, but it is known that it is started by the SUV adsorption to the hydrophilic surface. This is followed by the deformation and rupture of the vesicles, which triggers the vesicle fusion. These fused SUVs organize themselves to the planar supported bilayer structure (Fig 6 a). [44]

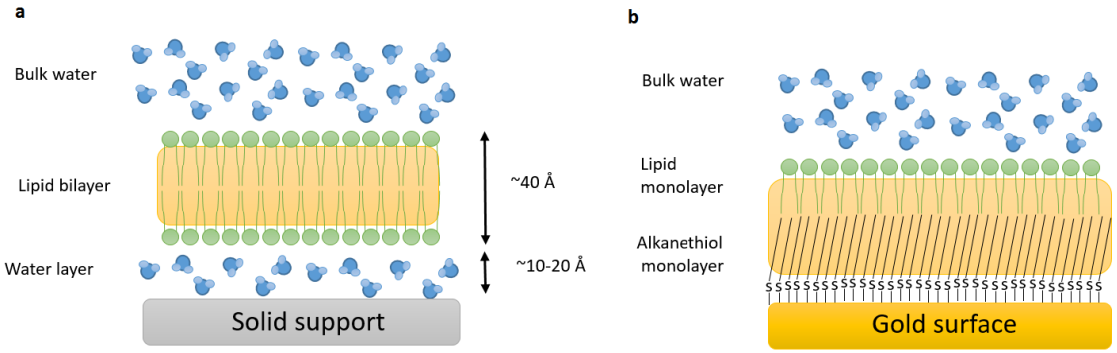

Figure 6: Schematic presentation of a) Supported lipid bilayer and b) hybrid bilayer. Again the hydrophobic areas are highlighted with light yellow colour. Adapted from Ref: [44]

Substrates that are not suitable for SLB formation such as gold, can be modified to form so called hybrid membranes (Fig. 6 b). In this method hydrophobic molecules are attached to the substrate crating a surface where a phospholipid monolayer can be formed. One of the methods is to attach alkane thiols to the gold surface. [44] This method introduced in Section 2.4.

2.2.2 Lipid-Protein Interactions

Lipid bilayer is the core of al biological membranes such as plasma membrane surrounding the cell. This membrane contains hundreds of different kinds of lipids, which are related to specific membrane functions [36]. Lipid membranes can influence to the protein conformation and its oligomerization state, like proven with multiple studies of enhanced peptide aggregation in membrane environment [2–4, 22]. The lipid membrane has an ability to vary its phase state, bilayer curvature and elasticity, surface charge, and degree of curvature. In addition to these physiochemical characteristics, the exact chemical nature of membrane lipids arising from such as acyl chain unsaturation, conformation and dynamics of lipid head groups and acyl chain and protein-lipid selectivity play a role in controlling the lipid-protein interaction. [45]

Studies with different amyloidogenic peptides show that anionic phospholipids, such as PS, PA and PG, represent the main membrane component responsible for enhancement of fibril formation. This behaviour is observed with multiple peptides, such as α–synuclein [2], Aβ [3], Temporin B [46] and IAPP [4]. This is why lipid bilayer is considered to act as an effective catalyst of amyloid fibrillogenesis. Thus, providing a generic environment where protein molecules adopt conformation and orientation promoting their assembly into protofibrillar and fibrillary structures. [47–50]

in addition, negative lipids can promote the amyloid formation by increasing the local concentration of the peptides [6].

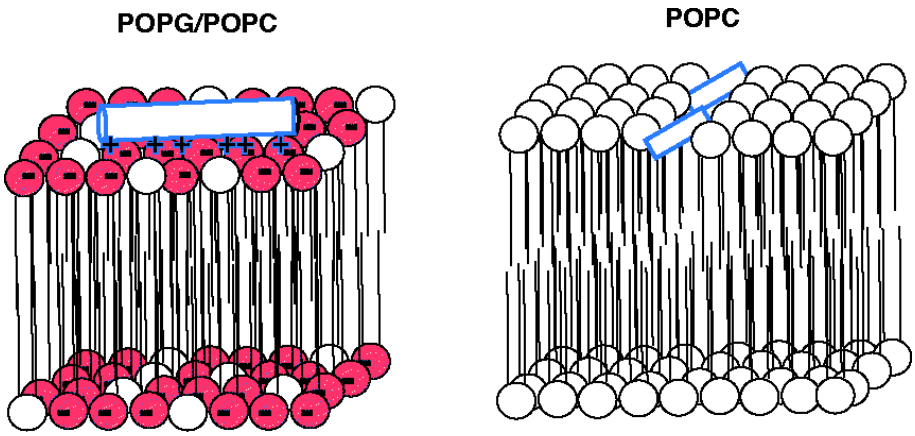

Figure 7: The effect of negative phospholipids in organization of KIGAKI aggregates. Adapted from Ref: [51]

Similarly, acidic POPG has shown to have important role in forming proper β-sheet secondary structures for cationic peptide KIGAKI (Fig. 7). It is argued that KIGAKI causes phase separation and leakage to the phospholipid membrane [51, 52]. However, in NMR studies with pure POPG bilayers, no phase separation was observed [53].

Furthermore, amyloids are known to possess an ability to extract membrane lipids [49, 50]. This may be the cause of membrane permeabilization and cell death in amyloidosis. [54]

2.3 Fluorescence

Fluorescence is emission of light emitted by a molecule upon excitation, collectively called fluorophore. This emission happens due to excited state that has followed an absorption of light. In excited state electron has moved from ground-state to a higher energy state. When the electron returns to the ground-state, photon is emitted.

Typically fluorophores are aromatic molecules. For almost all organic fluorophores the average time the fluorophore spends in excited state (i.e. lifetime) is between 1 and 10 ns. However, some exceptions exists including pyrene, which has displayed nearly 400 ns lifetime in degassed organic solvents. Pyrene consists of four fused benzene rings (Fig. 8 a), thus having hydrophobic nature. [55] The emission spectrum of pyrene is highly sensitive to solvent polarity. Hence, it has been employed to determine polarity in the vicinity of the fluorescent probe. Another property of pyrene is the formation of form an exited dimer 'excimer' when pyrene molecules are close enough. Pyrene excimer follows a collision between an excited monomer and a ground state pyrene, which is possible due to the unusually long lifetime of pyrene emission. [56] This excimer emission appears as an unstructured band at

longer wavelengths centred proximity 470-480 nm [55]. A typical emission spectrum has high monomer peaks (378 nm and 398 nm) and broad the excimer band (Fig.8).

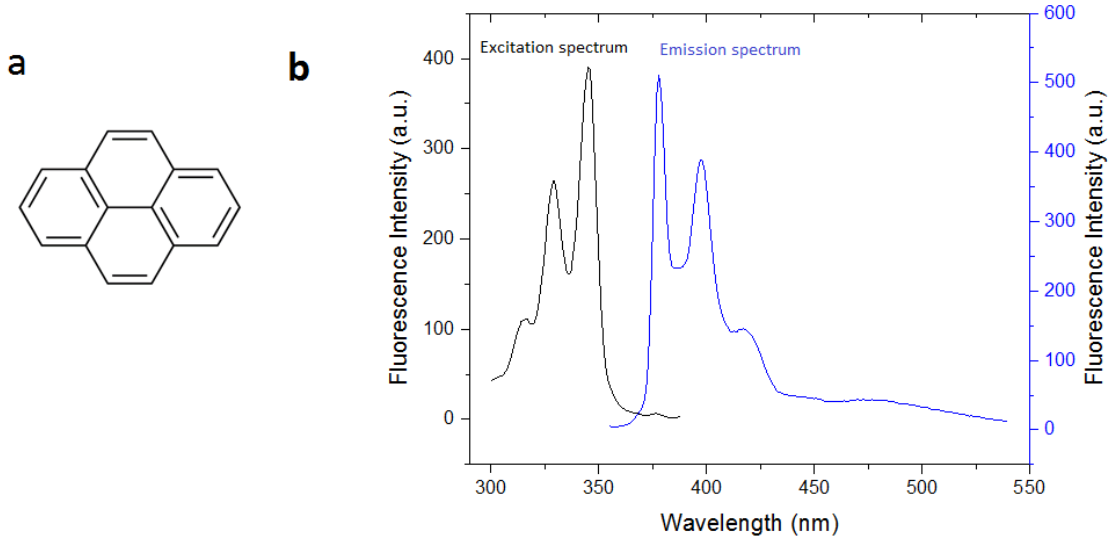

Figure 8: a) The structure pyrene. b) Typical excitation (—) and emission (—) spectrum of pyrene.

Due to these unusual properties, pyrene is a frequently used lipid-linked fluorophore. Pyrene lipids are used in studies of biophysical phenomena such as lateral diffusion, inter- or transbilayer movement of lipids and lateral organization of membranes. In addition, protein binding to membranes, lipid conformation and the activity of lipolytic enzymes are wildly studied with employing pyrene lipids. However, pyrene lipids have some disadvantages. These include the relatively large size of the fluorophore and the requirement of UV-excitation, which is not feasible with all microscopes [57].

Pyrene is usually attached to the end of acyl chain in sn-2-position. Its' 'width' is approximately twice the width of an aliphatic chain. In addition, the polycyclic aromatic ring structure is much more rigid than a saturated alkyl chain. Thus, despite its hydrophobic nature, pyrene moiety can significantly change the properties of the labelled lipid. [57]

There are multiple different methods that utilize the phenomena of fluorescence, including fluorescence spectroscopy, fluorescence microscopy, fluorescence anisotropy, absorbance spectroscopy fluorescence, and lifetime measurements [58]. The two fist methods are also applied in this thesis.

In fluorescent spectroscopy the shift of an emission intensity or spectrum can be observed. These observations are clues to the change of conformation or environment of the investigated molecule. For example, if the emission of pyrene excimer is increased, it suggests that more pyrene molecules are close to each other. Another example are the amyloid specific dyes. If the intensity of ThT is measured during the

amyloid formation, kinetics of the formation can be recorded resulting a sinusoidal curve (Fig. 2) [23] . From the curve the different phases, such discussed earlier (Section 2.1.1), can be then identified and analysed [30, 31]. If the fluorescence is in the visible region, the fluorescence signal can be used to record an image. This fluorescence brings otherwise invisible, too small or transparent, particles to our sight. This is utilized in fluorescent microscopy.

2.4 Self-Assembled Monolayers and Alkylation

Sometimes there is need to change the surface properties of the used system. This is when self-assemble monolayers (SAMs) become useful. These are molecular assemblies formed spontaneously on surfaces by adsorption. [59]

The most studied SAMs are the alkanethiol monolayers. Alkanethiols are group of molecules that contain alkane tail and sulfhydryl (–C–SH or R–SH) group. They are known from the tendency to create highly ordered monolayer structures onto gold and other noble metal surfaces. [60, 61]. Only by varying the head group of the alkanethiol, the surface properties of the monolayer can be controlled. This is why alkanethiol SAMs have applications in great variety of fields such as: surface wetting, non-fouling property, electrochemistry, surface passivation, protein binding, DNA assembly, corrosion resistance, biological arrays, cell interactions, and molecular electronics [62].

Multiple driving forces has been identified to be responsible to this assembly. Firstly, the gold-sulfur affinity is order of 45 kcal/mol, thus forming a semi-covalent bond [63]. Secondly, alkane chains experience a hydrophobic interaction in water solution. Thus, this Vander Waals interaction forces the alkyl chains to tilt in order to maximize the chain-chain interaction and lower the overall surface energy. If the carbon chains are over 10 carbons in length, the hydrophobic interactions between the chains overcomes the rotational degrees of freedom and a well-ordered monolayer can be formed. [64]

A preparation of thiol monolayer is usually a simple, but time consuming process. Traditionally alkanethiol monolayers are created by incubating the gold surface in a thiol solution for a night. However, it is shown that a flow of thiol solution through microfluidic channel can create a SAM layer on a gold surface within seconds [65].

Like discussed in Section 2.2.1 a lipid monolayer can be formed on top of a self-assembled alkanethiol monolayer to create a hybrid bilayer. There are a wide variety of alkanethiols that can be used for this purpose. However, octadecanethiol is typical choice for hybrid bilayer formation due its ability to form tightly packed well-ordered monolayers. The hybrid bilayer is prepared onto alkanethiol monolayer by vesicle fusion of liposomes similarly to SLB. [44]

2.5 Microfluidics

Microfluidics (mf) is a study and manipulation of fluids (liquid and gases) at sub millimetre length scale. At such small length scales physical phenomena manifest differently than in a macro scale. For example, the force due to gravity at length scales of microfluidic channels is negligible, but the surface forces are dominant. In addition, the flow of fluid behaves different than in macro scale. In micro scale viscous forces are dominant against inertia forces, thus causing fluid flow to be laminar instead of turbulent. [66] In laminar flow, diffusion is the only force that promotes mixing of the fluid molecules. These differences of physical phenomena in microsystems must be considered in designing a chip. Thus, if additional mixing is needed, turbulence must be enhanced by channel geometry (Fig. 9) or using grooves in channels [67].

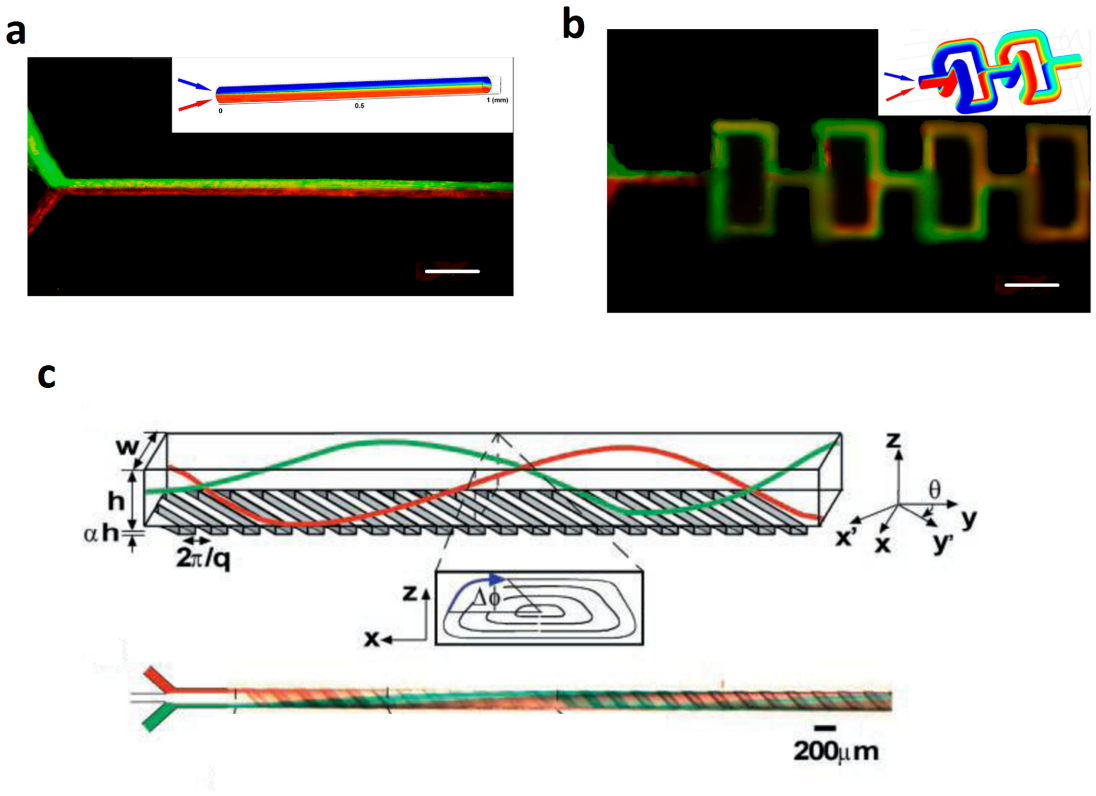

Figure 9: Mixing in a microfluidic device. a) Two streams of different dyes flowed through a straight microfluidic channel. b) Mixing can be enhanced by 3D geometry of the channel or c) grooves in channel floor. Adapted from Ref: [68] and [69]

2.5.1 Physics of Microfluidic Environment

The change in fluidity properties when scale is decreased is characterised by dimensionless numbers such as: Reynolds, Péclet and Bond number. Reynolds number describes the relationship of inertial and viscous forces and can be written by equation:

$$Re = \frac{\rho v L}{\eta}, \tag{3}$$

where ρ stands for the density and η the viscosity of the fluid, v is the velocity of the flow and L the characteristic length of the channel. In a bulk flow the inertial forces are dominant, hence the fluid flow is turbulent. However, when the scale is smaller, the value of Reynolds number degreases. When Re reaches a value below 10, the physics of fluid changes and the flow of liquid is laminar. If $10 < Re < 2000$, flow is considered to be something between laminar and turbulent. [70]

Péclect number shows that diffusion dominates advection in small scale. It is described by equation:

$$Pe = \frac{vL}{D}, \tag{4}$$

where D stands for diffusivity that can be calculated to ball shaped molecule with the radius of r by: D $\approx k_B T/6\pi\eta r$. In small scales the numerator of the Péclect number is equation, corresponding the advective transport rate, becomes negligible compared to diffusive transport rete in nominator. [70]

In addition to advection the force due to gravity becomes negligible in micro scale. This is when the surface forces start to dominate. The ration of gravity to surface forces is represented by Bond number:

$$Bo = \frac{\rho a L^2}{\gamma}, \tag{5}$$

where a is the acceleration due gravity and γ surface tension. [70]

2.5.2 Used Materials in Microfluidics

Various different materials can be used for preparing microfluidic devices, including: silicon, glass, plastics and even paper (Fig. 10). The first microfluidic devices were fabricated by etching silicon [71]. However, due to the demand for high-end facility and costly microfabrication processes for silicon etching, new ways to fabricate microchannels where needed. In chemical analyses glass and plastics have been the most popular materials. This is due to their electrically insulating properties, thus allowing the separation of analyses. In addition, the transparency of these materials enables the observation of the experiments using conventional microscopes. However, due to the expensiveness and brittleness of the glass, polymers are chosen over glass in many applications. [72]

The most used polymer is polydimethylsiloxane (PDMS), PDMS is the dominant material in recent publications. [72] This is mainly due to its properties that enables

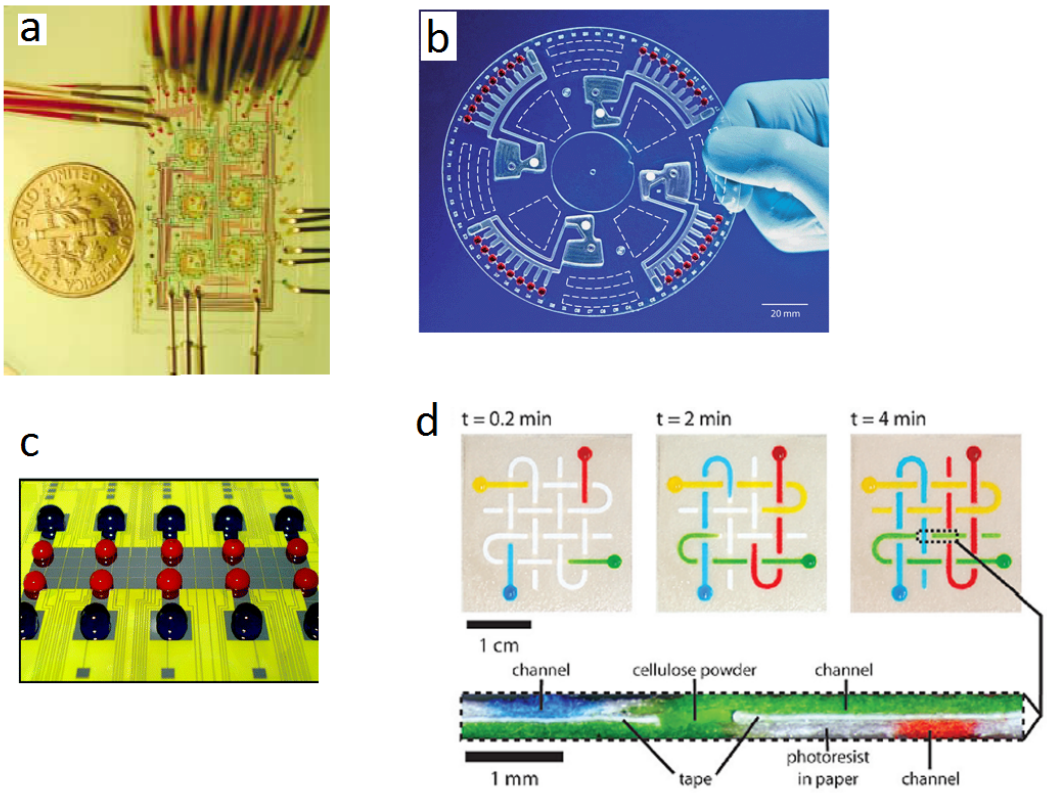

Figure 10: Examples of different microfluidics devices: a) Multilayer PDMS chip sealed with glass. The flow of fluid is produced by pressure. b) A circular disc PDMS device, which is designed for centrifugal microfluidics. c) Digital microfluidics chip, where fluid droplets are moved by electrowetting, d) Paper-based microfluidic device made by stacking two layers of patterned paper and one layer of double-sided adhesive tape. Adapted from ref: [73], [74], [75] and [76]

rapid and inexpensive replica moulding with feature size as small as 2 nm. In addition, PDMS has low glass transition temperature, high free volume and porosity. Thus, resulting high flexibility. [77] This property is used as an advantage in two layered microfluidic applications, where a thin PDMS membrane between two channel layers can be deflected up and down applying pressure. Hence, flow can be controlled by using the membrane as valve or multiple sequential valves as a pneumatic pump. [78]

As downside the properties of PDMS are responsible for its significant vapour and liquid diffusion properties [77]. Although this can cause serious problems in some applications, porosity is also used as advantage in devices such as membrane application for vapour separation of volatile gasses [79].

The channels in microfluidic devices are usually sealed with a microscope glass. If compatibility with UV-light is required, a quartz substrate is preferred due to the low absorption of UV-wavelengths of light. Quartz has a negative surface charge in high pH and positive when pH drops under 2–3.7. [80] These hydrophilic surfaces

are also good substrates for SLB formation [81]. There are previous publications reporting SLB formation in microfluidic chips by vesicle fusion [82, 83]. However, no studies for amyloid formation in mf-chip with a supported lipid bilayer have been published yet.

2.5.3 Microfluidics in Amyloid Research

Although the majority of work concerning *in vitro* amyloid formation are conducted in bulk systems, there is an increasing number of papers describing the formation and detection of amyloids in microfluidic systems [12–16, 84]. The detection is mainly performed by employing amyloid binding dyes such as Thioflavin T. [12–14, 16]. For example, ThT fluorescence was applied in microdroplet assays enabling the detection and independent quantification of both primary and secondary nucleation events in amyloid formation [16]. The detection of these two events was only achieved by reducing the system size below a critical value of operating microfluidics. Another interesting example of amyloid detection is the microfluidic biosensor application for the detection of Aβ(1-42) amyloids [15]. By employing microfluidics and cyclic voltammetry the work tackled the problem of current methods, which have time-consuming, expensive, and labour intensive amyloid detection.

The previous examples show how microfluidic environments allow new strategies to conduct experiments, but this unique environment can also affect the investigated system. Firstly, has been reported that higher flow rates can affect the aggregate morphology. Specifically, bovine insulin has been shown to form spherical aggregates (amyloid spherulites) at low flows rate, and thin fibrils at high flow rates, consequentially. Secondly, the fibrils tend to align with the flow. However, this effect was seen mainly in the central part and the edges of the channel. [84] In addition to the morphology of the fibrils, flow has been seen to affect the rate of the fibril growth [12]. Another experiment with insulin peptide and continuous flow reported an amyloid deposition starting at the centre of the channel, followed by a considerably high deposition at the side walls. In addition, the experiment revealed that the density of fibrils higher in mf-chamber than bulk. This is most certainly caused by the availability of continuous flow of fresh monomers and the high surface to volume ratio provided by the micro-chamber. [12]

It is also suggested that microfluidics has a great potential to work as a high-throughput analysis platform for amyloid studies [13, 14]. A novel microfluidic analytical method for evaluating inhibitory effect of 12 small molecules against on Aβ aggregation applying ThT fluorescence is reported with encouraging results [13]. The same system was used to investigate the dissociation and clearance of Aβ aggregates [14].

3 Materials and Methods

In this section used materials and chosen methods are introduced. To start with, employed peptides and lipids are listed, and sample preparation is described. This is followed by a brief introduction to the experiment set-up. In addition, different parts of the set-up is discussed more profoundly. Particularly the preparation of a microfluidic chip is covered. Finally, the two methods for amyloid formation and detection are presented.

3.1 Materials and Sample Preparation

The materials used in amyloid characterization experiments were synthetic organic compounds. They were purchased as clean powders and stored in freezer conditions. The peptides used for amyloid formation: Amyloid-β(1-42) peptide (Aβ) [85], $[KIGAKI]_3$-NH_2 (KIGAKI) [86, 87], Poly-lysine ($PolyK_10$) [88] and Temporin B (TempB) [22] were chosen based on their tendency to form β-sheet rich aggregates/amyloid fibrils. KIGAKI is highly cationic and can be readily expected to interact strongly with acidic phospholipids.

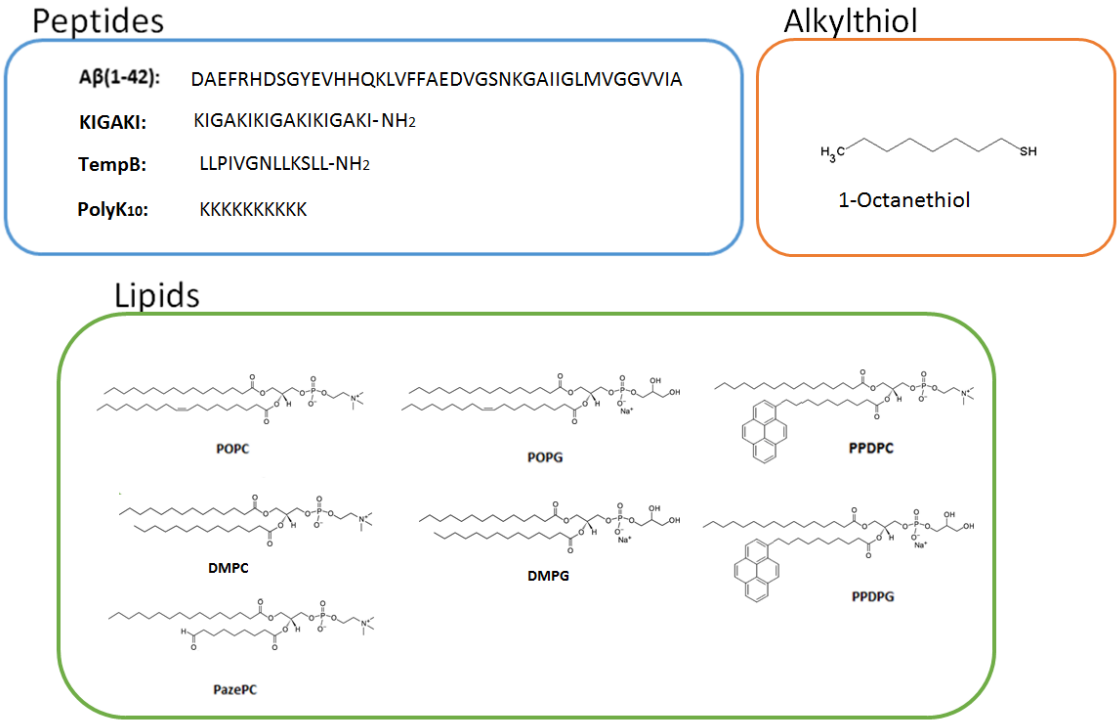

Figure 11: The amino acid sequences of peptides used, structures of applied lipids, and alkylthiol.

Lipids were zwitterionic 1-palmitoyl-2-oleoyl-sn-glycero-3-phosphocholine (POPC), acidic phospholipids 1-palmitoyl-2-oleoyl-sn-glycero-3-phospho-(1'-rac-glycerol) (POPG),

and 1-palmitoyl-2-[10-(pyren-1-yl)] decanoyl-sn-glycero-3-phosphoglycerol (PPDPG), (1-palmitoyl-2[6-(pyren-1-yl)]decanoyl-sn-glycero-3-phosphocholine)(PPDPC), and oxidized phospholipid derivative (ox-pl) 1-palmitoyl-2-azelaoyl-sn-glycero-3-phosphocholine (PazePC). The fluorescent phospholipid analogs PPDPG and PPDPC were included to allow the observation of lipids in the lipid-protein aggregates.

Lipids were purchased as a powders and dissolved in chloroform. These stock solutions were stored in $-20°C$. The concentrations were checked either gravimetrically (POPC, POPG and PazePC) or by absorbance (PPDPG and PPDPC). In gravimetric assay small amount of stock solution was dried to in advance weighted aluminium pans under N_2 flow. The drying was completed holding the pans in a vacuum for at least 5 hours. Then the pans were weighted and the mass of the dry lipid can be calculated by extracting the weight of the empty pan. When molar weight of the lipid, volume and mass were known, the concentration were determined with a simple calculation. The stock concentrations of lipids with fluorescent probe can be measured from the absorbance of the fluorescent molecule. This was performed by diluting small amount of stock solution to ethanol and measuring the absorbance spectra. For pyrene, the absorbance of 342 nm was defined and concentration of the stock was calculated from a simple relation:

$$C = x * \frac{A_{342nm}}{\varepsilon * Opt} \tag{6}$$

where x is the dilution factor, A_{342nm} is the absorbance of 342 nm wavelength in ethanol, ε is the extrinsic constant, which is 38 000 for pyrene lipids in ethanol, and Opt is constant related to the cuvette used in the measurement.

Both lipid and peptide samples were diluted in a suitable buffer or DI-water (ultra-pure MilliQ-water). Buffers were made by weighing appropriate amount of HEPES (4-(2-hydroxyethyl)-1-piperazineethanesulfonic acid) or MES (2-(N-morpholino)ethanesulfonic acid and EDTA (Ethylenediaminetetraacetic acid) and dissolving to DI-water. The dissolving was performed with the help of magnetic stirrer. After letting the buffer agents to dissolve for few hours, the pH of the buffer was adjusted with HCL/KOH and monitored by pH/conductivity meter. Two different buffer mixtures were prepared: pH 7 buffer with 20 mM HEPES and 0.1 mM EDTA, and pH 4 buffer with 50 mM MES and 0.1 mM EDTA.

These buffers were used to dilute the liposomes and peptides to desired concentration. The preparation of liposomes and peptide solutions are described next.

3.1.1 Liposome Preparation

Liposomes form upon introducing lipid molecules into an aqueous environment. Dry lipid films form large multilamellar vesicles (MLV) after addition of aqueous phase followed by mechanical agitation provided by vortexing, shaking, swirling or pipetting.

If unilamellar (ULV) or smaller liposomes are desired, energy has to be brought into the system. [89]

The two most frequently used methods for disturbing MLVs are by extrusion through pored filters or by ultrasound. The former involves loss of material in the filters as a major drawback. Accordingly, ultrasound was used in this work by employing adaptive focused ultrasound (AFU). In focused ultrasound the sample is placed it the focal point of the ultrasound waves created by a transducer. These sound waves produce pressure gradients, which results in a formation of gas bubbles as cavities. If the cavitation bubble collapses mechanical energy is released in the form of secondary shock waves, thus producing high temperature hot spots or continuous oscillations. The cavitation and secondary shock waves can cause random shattering of large MLVs into small lipid bilayer fragments. These are believed to assemble into thermodynamically stable, smaller unilamellar vesicles. [90]

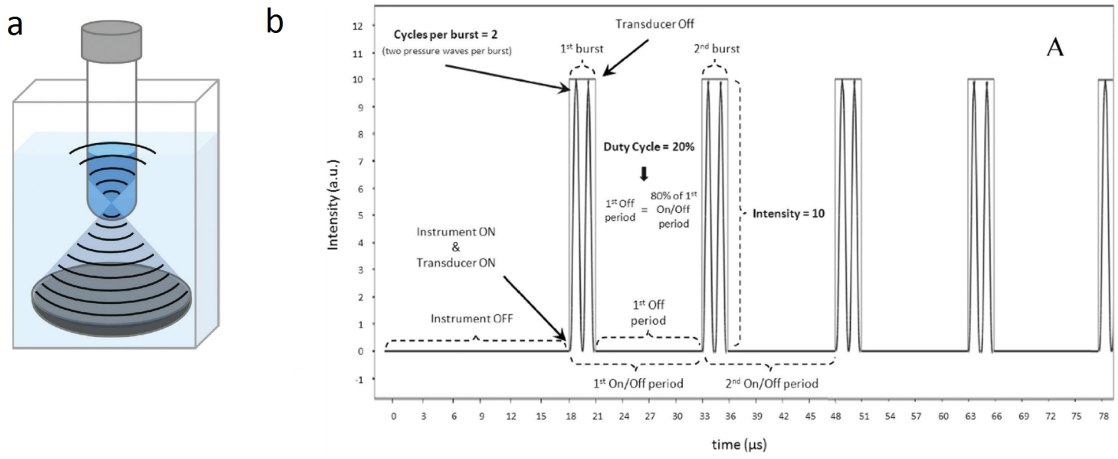

Figure 12: a) Schematic illustration of the AFU acoustic field during ON period in the transducer. The transducer and the sample are in a thermostated water bath. B) Schematic illustration of the AFU transducer output applying parameters: intensity 10, CPB 2 and DC 20%. Adapted from ref: [90]

The size of the liposomes can be controlled by changing the applied parameters in AFU. These parameters include: duty cycle (DC), Cycles per burst (CPB), Intensity and treatment time (Fig. 12 b). DC means the percentage of the time where transducer is "On", thus modulating the duration of the pressure wave bursts and the relaxing time between two successive bursts. CPB means the number of waves in one burst. In other words, if CPB is chosen to be 2, every time the transducer is on, two pressure waves is transmitted. The amplitude of the acoustic pressure is controlled by a parameter called intensity, meaning the acoustic power transmitted by transducer per unit area. The treatment time simply corresponds the duration of the sonication procedure. Time is seen to correlate to the mean size and polydispersity of the vesicle solution. [90]

In this thesis, the lipid powders were dissolved in a chloroform to create stock

solutions and stored at -20 C. Appropriate aliquots of stock solutions were taken with Hamiltton syringes to a glass tubes. The solvent was removed with placing tubes under N_2 flow, following maintains of the lipid samples in vacuum for at least 2 hours. The dry lipids were hydrated to final concentration of buffer or DI-water by vortexing vigorously, followed by sonication. Parameters used in sonication varied for different lipid solutions. Solutions without pyrene were treated by 30 min with Duty Cycle: 10 %, Intensity: 7, Cycles per Burst: 100, using power track maintaining temperature near 25 °C. If lipids included 20 per cent of pyrene analogues additional 20 min sonication with CPB increased to 200 was needed. For pure pyrene-lipid solutions the sonication time was increased to 1.5 hours. The sonication resulted a uniform solution of SUVs with average size near 50 nm with most lipid samples. However, the smallest average size achieved for PPDPC:PPDPG solutions was 1000 nm. The size of the liposomes where measured with dynamic light scattering (DLS)

3.1.2 Peptide Preparation

The appropriate amount of the peptide powder were weighted with SuperG scale and dissolved in DI-water (TempB), 20% acetonitrile (KIGAKI and PlyK10) or 90% DMSO (Aβ peptide) to yield 50 μM solution. These solutions were diluted prior to the experiment with pH 7 buffer or DI-water to a final concentration of 0.4 μM. In addition, the Aβ solution was filtered by a syringe filter with 0.2 μm pores.

3.2 Experiment Set-Up

This thesis applied experimental methods that were unique in the way that no commercial system fulfilled all the requirements. This is why the experiment set-up was constructed from multiple devices, which either worked as a template for the experiment or produced data from the measurements. A box-diagram depicts all the components of the set-up (Fig. 13).

The whole set-up was built around an inverted fluorescent microscope. The experiments were conducted on a microscope stage in a microfluidic chip. This chip was designed and fabricated for the purpose of these experiments. The control of sample flow was accomplished with regulating pressure in sample reservoirs and control channels. Images (video and still) were recorded with Hamamatsu C4742-95 CCD and Canon EOS 10 D cameras. In addition, impedance data were recorded with impedance measurement system.

Hence, by employing this system, two different form of data was achieved: images and impedance data. These two data-types serve the basis of two different characterization methods: visual (images) or electronic method (impedance data).

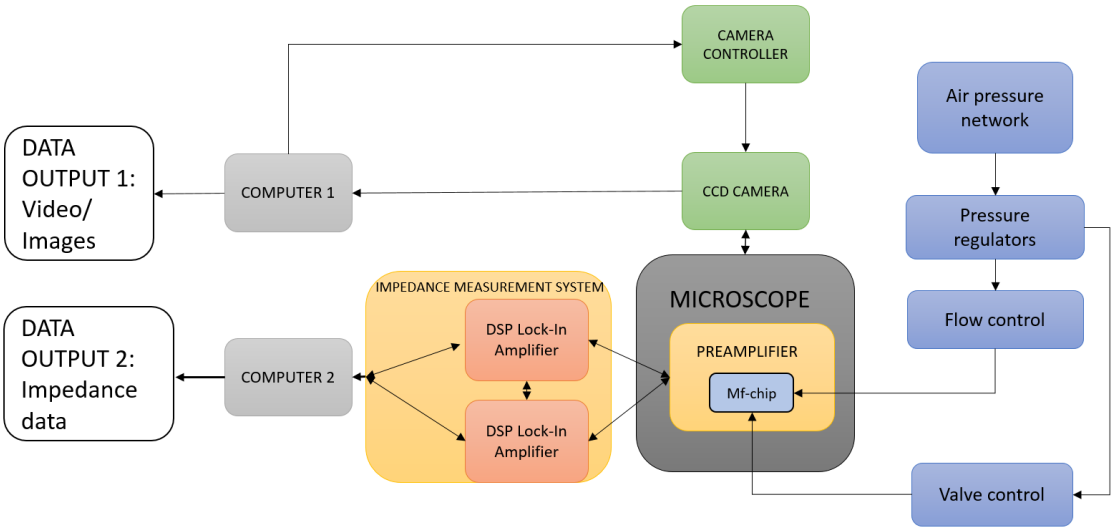

Figure 13: Box-diagram of the experiment set-up.

3.2.1 Fluorescence Microscopy

One way to detect fluorescence emission is to use a fluorescence microscope. With the help of suitable filters emission wavelengths and excitation wavelengths can be chosen. The filters are named either as short pass (SP), band pass (BP) or long pass (LP) according to its properties. SP filter is designed to pass wavelengths shorter than the given value. BP filter pass given range of frequencies and LP filter all longer wavelengths consequently. [91]

In this thesis an Olympus IX70 inverted fluorescence microscope with USHIO USD-102D mercury lamp was employed, with following fluorescence filters: Olympus NBV filter cube with excitation BP420-440 nm and LP475 nm emission filter, WIG filter with BP530-550 nm excitation and LP580 nm filter, and WIBA filter BP460-495 nm excitation and BP510-550 nm emission filter (Table 1.). One fundamental notion is that the excitation intensity varies by wavelength in mercury lamps (Fig. 14). NBV and WIG filter have excitation wavelengths that include a peak of the lamp spectrum. However, WIBA has the excitation band pass (BP) in low intensity region of the lamp spectrum.

Table 1: Fluorescence filter cubes used in this work (BP = Band pass, LP = Long pass)

Filter	**Excitation**	**Dichroic Mirror**	**Emission**
NBV	BP420-440 nm	455 nm	LP475 nm
WIBA	BP460-495 nm	505 nm	510-550 nm
WIG	BP530-550 nm	570 nm	LP580 nm

The relative intensity of the fluorescence images were quantified by ImageJ software

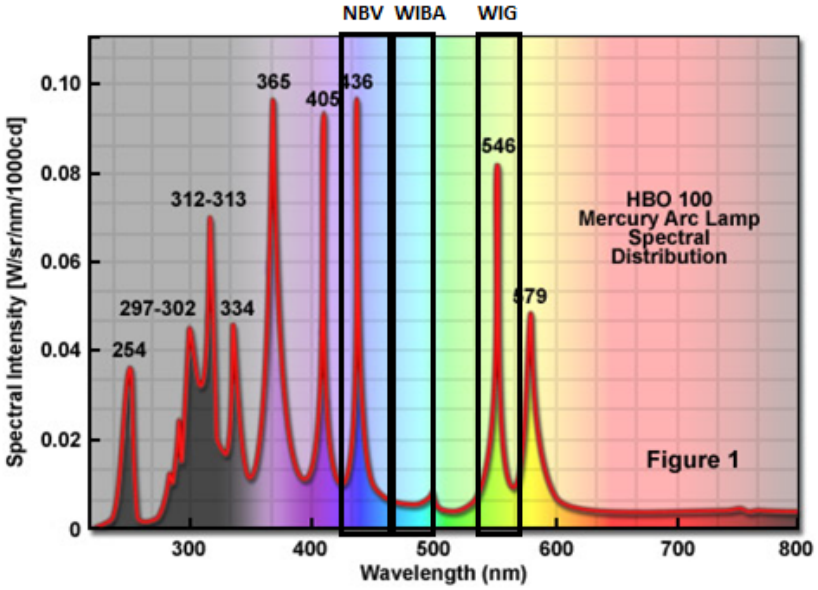

Figure 14: Spectral content of the mercury arc light output and NBV, WIBA, and WIG excitation filter bands featured. Adapted from Ref: [92]

and the Intensity-Distance graphs were plotted with Origin.

3.2.2 Impedance Spectroscopy

Impedance data was recorded with Two DSP SR830 Lock-in amplifiers (DSPamp) preforming four-terminal sensing (4T sensing) from the microfluidic chip (Fig. 15). 4T sensing was chosen as the measurement method since it eliminates wire resistances, resulting better sensitivity for low resistance values compared to two-point measurements [93]. The DSPamps were connected to the computer employing a common port to obtain a simultaneous computer control. In addition, a mutual reference signal was applied to the DSB Lock–In amplifiers. Other DSPamp was used to generate AC voltage between the outer electrodes (e1 and e4 in Fig. 15) and a voltage drop was measured between the inner electrodes (e2 and e3 in Fig. 15 b). The voltage drop signal was passed through a pre-amplifier circuit assembled to the perimeter of the mf-chip. The experiments were controlled and recorded with LabVIEW software.

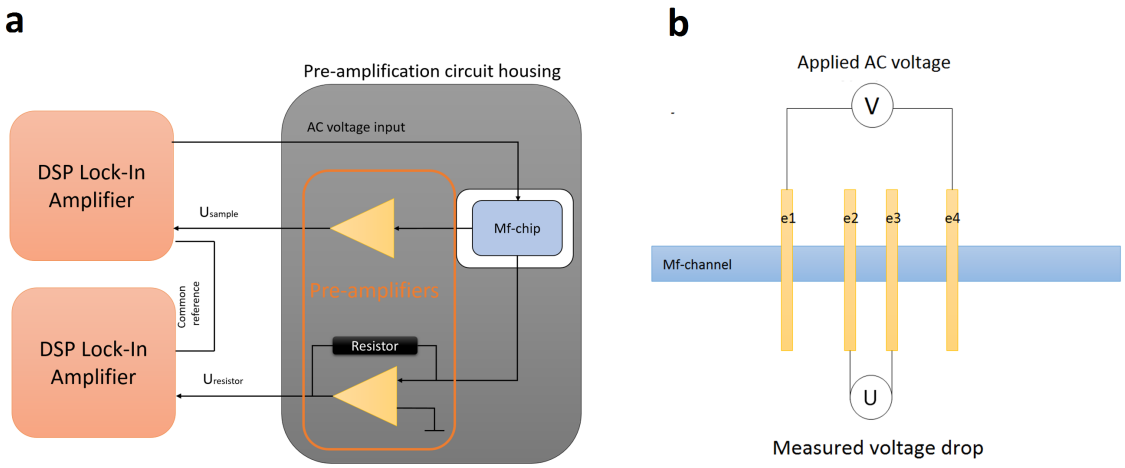

Figure 15: a. A box diagram from the impedance measurement system with two Lock-In amplifiers, microfluidic chip and pre-amplifiers. b. In a four-terminal sensing measurement AC voltage (V) was applied to the outer electrodes (e1 and e4). The resultant voltage drop (U) was measured between the electrodes e2 and e3.

In addition to voltage drop, current passing through the sample and phase shift were measured. The current was determined by a virtual ground connection where the voltage drop across a resistor with known value was monitored. The corresponding current was calculated using Ohm's law:

$$I = \frac{U}{R}, \tag{7}$$

where I stands for current, U voltage drop, and R the known resistance.

Since the sample is a complex conductor and it cannot be characterized with a simple resistor, imaginary components such as capacitance (C) and inductance (L) has to

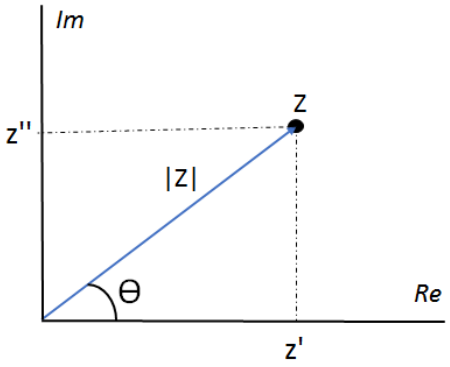

Figure 16: Graphical illustration of inductance in Cartesian coordinates.

be added to the equation. Consequently, the measured quantity is the sum of real part: resistance (Z'), and imaginary part: reactance (Z"). The sum of resistance and reactance is called impedance (Z):

$$Z = Z' + jZ''. \tag{8}$$

This can be visualized in Cartesian coordinates (Fig. 16), where reactance is the y-axis, resistance is the x-axis, and the impedance is the length of the corresponding vector. Reactance can be further replaced with capacitance:

$$Z_C = \frac{1}{j\omega C} = \frac{1}{\omega C} e^{-j\frac{\pi}{2}}, \tag{9}$$

or/and inductance:

$$Z_L = j\omega L = \omega L e^{j\frac{\pi}{2}}. \tag{10}$$

From the polar forms we can see that in case of an applied sinusoidal voltage, the resulting sinusoidal current is 90 degrees out of phase with the voltage. Hence, in an inductor, the current is lagging and in a capacitor the current is leading.

The values measured with lock-in amplifier are the magnitude of the voltage drop and phase:

$$U = \sqrt{X^2 + Y^2} \tag{11}$$

$$\theta = arctan(\frac{X}{Y}), \tag{12}$$

where X means the 'in-phase' component and Y the 'quadrature' component. Applying this measured voltage drop and defined current to the Equation 7 and additionally replacing R with Z, sample impedance can be calculated. Thus,

$$Z = \frac{U}{I}. \tag{13}$$

The Lock-in Amplifier allows to vary both the amplitude and the frequency of the input signal. The measurement started with monitoring the conductivity changes during the organization of the sample. During this 1 V input signal was applied with frequency of 777 Hz. After the voltage drop and current had reach plateau, voltage and frequency characteristics of the sample was measured by varying the input signal. In frequency characteristic measurements 0.4 V signal with frequencies from 33 Hz to 4000 Hz were applied. Similarly, when defining voltage characteristics, 344 Hz frequency with increasing voltage from 0.1 V to 1.6 V was used.

The impedance measurement system displays the signals as root mean square values (RMS). The relationship between signal amplitude and RMS value for sine wave is:

$$Amplitude = \sqrt{2} * RMS. \tag{14}$$

Thus, all the voltage and current values in this thesis are in RMS values.

3.3 Chip Fabrication

Microfluidic chip was chosen to serve as the platform of this thesis due to possible miniaturization and customization of the experiment environment.

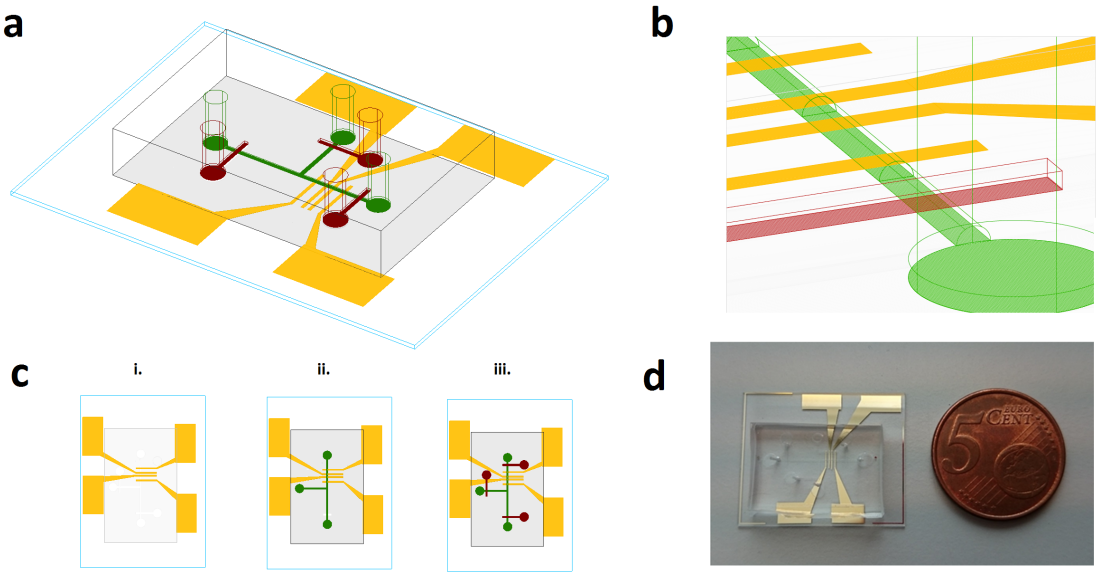

Figure 17: a) A CAD model of the microfluidic chip with Au/WTi electrodes on the quartz substrate. b) Zoomed view from control channel crossing the flow channel. c) Different layers of the device: substrate layer with the electrodes, the flow layer plasma bonded to the substrate and control layer that is thermally bonded to the flow layer. d) Photograph of a finished device. The schematic figures are not in scale for sake of clarity.

The microfluidic chip consisted of two main parts: the PDMS channel structure and the electrode/quartz substrate that seals the fluid channel. The channel structure

was in two layers including a control (upper) and flow (bottom) layers. Both of these layers are fabricated separately and bonded together to create pressure controlled valves on the fowl layer. This kind of structure was introduced in: Ref [78].

A 3D CAD illustration of the chip is provided (Fig. 17 a), where the channel and electrode structures can be seen. Control channels (red coloured) in the upper layer cross a flow channel (green coloured) with a semicircular cross-section (Fig, 17 b). The semicircular cross-section is needed to the proper function of the valves [78]. At the bottom of the device there is quartz substrate with Au/WTi electrodes (Fig. 17 c, i). These surface electrodes had width of 100 μm and height 70 nm. The distance between central electrodes was 300 μM. However, the distance between outer and its adjacent central electrode was 450 μM. The flow channel was created by bonding the flow layer and quartz substrate together (Fig. 17 c, ii). The top layer served as control layer with the dead ended channels. These channels were used as valves to control the fluid stream in the flow channel (Fig. 17 c, iii).

The finished chip (Fig. 17) was not much bigger than a 5 cent coin. Both, flow and control channels were 200 μm in width. However, the channel heights differed. Control channels were 50 μm high, but flow channel was only 9.7 μm. In addition to aforementioned semi-circular cross-section, shallow flow channel was required to ensure the proper valve function.

3.3.1 Electrode Fabrication

Au/TiW surface electrodes were fabricated on 100 mm thick fused silica (i.e. quartz) wafers. The fabrication processes were conducted in clean room facility of Micronova Nanofabrication centre of Aalto University. The electrodes were created using lift-off method. First, the clean wafers were treated with hexamethyldisilazane (HDMS) in HDMS prime oven to minimize water absorption to the surface (Fig. 18 1.). Hence, this ensured better adhesion of resist. The surface treatment was followed by a resist (AZ5214E) spin on the chip for 30 s with 3000 rpm (Fig. 18 2.) and bake in 95.5 °C for 1 min.

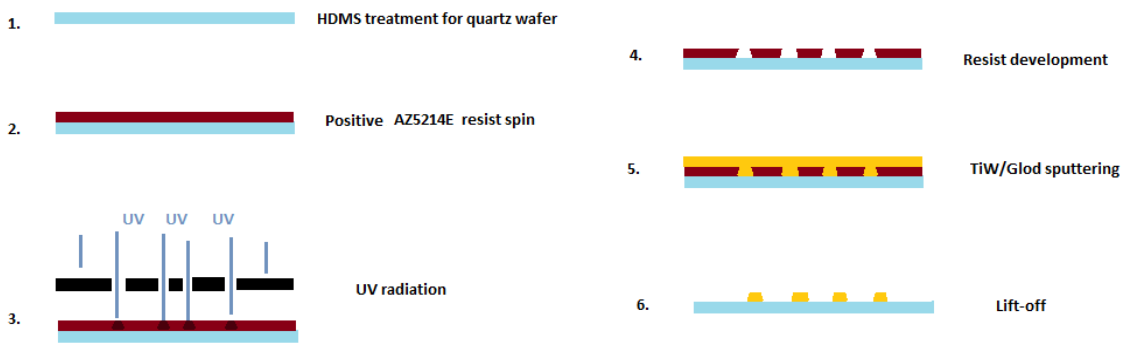

Figure 18: Schematic representation of the major microfabrication steps in a gold electrode deposition.

A negative pattern of the electrodes was created by exposing the resist surface trough a negative mask with UV light (Fig. 18 3.) The exposure was conducted in two phases. First, 1 s exposure with mask was conducted, followed by post exposure bake in 120.5 °C for 2 min. In the second exposure whole wafer was exposed for 5 s. The UV light changed the resist polymer structure so, that the areas exposed in both exposure phases were soluble in developer AZ-351b (Fig. 18 4.). The AZ5214E is a positive resist that creates negative slopes. In other words, it provides the same pattern that the applied mask has and the structures fabricated will have a negative wall profile, which makes the aggravated cross sections to resemble a cone. This wall profile is required for successful lift-off process. After patterning, TiW adhesion layer was sputtered on the wafer, followed by sputtering of Au layer (Fig. 18 5.). The adhesion layer is needed between the gold layer and the quartz surface, since noble metals has pour adhesion on quartz. The total thickens of the electrodes were approximately 70 nm. Due to the high solubility of the resist in acetone, the lift-off was simply conduced in acetone bath. To accelerate the process sonication was employed (6.). Finally the individual electrode substrates were cut from the wafer with dicing saw.

3.3.2 PDMS Moulding

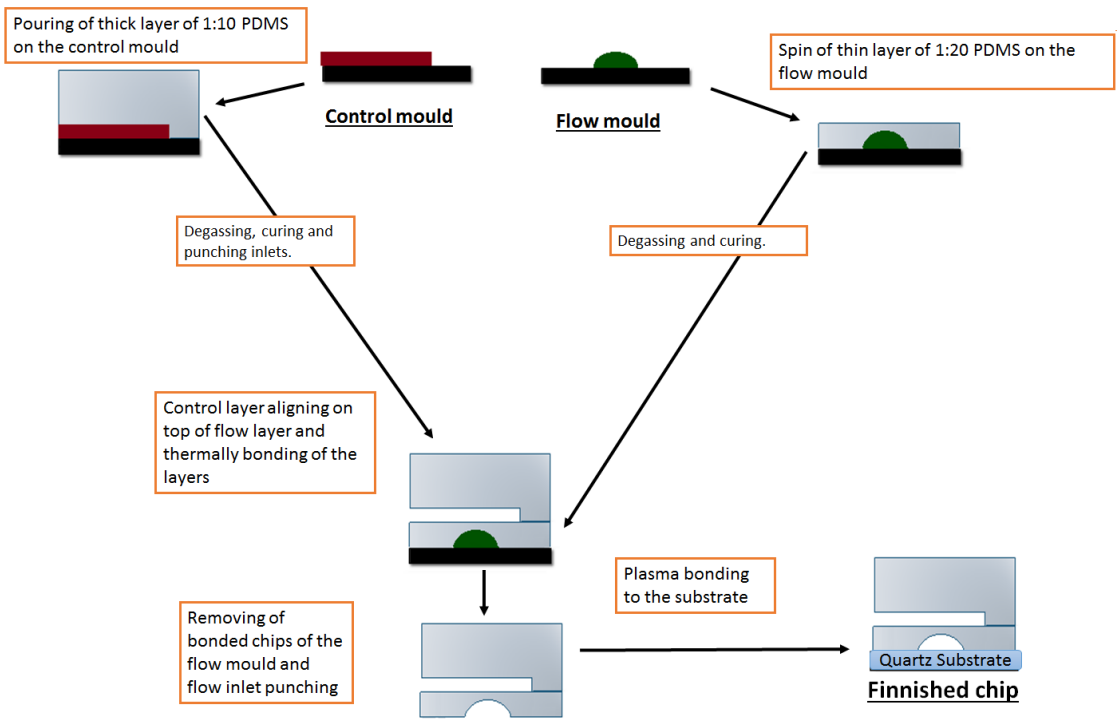

Figure 19: Schematic figure of the main steps of soft lithography for creating a two-layered PDMS device.

The channel structure of a microfluidic chip was fabricated with soft lithography of polydimethylsiloxane (PDMS), as described in: [78], with small modifications (Fig. 19). Microfabricated moulds for flow and control channels were used to create channel structures.

Two PDMS mixtures were prepared with a different curing agent:monomer weight ratios I) 40 g 1:10 and II) 10 g 1:20. The fist mixture was poured over the control layer mould. The second mix was spun in 2000 rpm for 30 s on to the flow mould to create a thin membrane. Bubbles created in PDMS mixing were removed by keeping both layers in vacuum. After the bubbles had been removed, both layers were cured in 80 $°C$ oven. The thicker layer was cured for 40 minutes (control layer) and thinner for 25 minutes (flow layer). The cured control layer was cut in to a pieces and sample inlets were punched before aligning individual control layers on top of the flow layer. The two PDMS layers were bonded together thermally in 80 $°C$. In order to create a good bond, at least 1.5 hour cure was required. However, overnight treatment was preferred. Next day the chips were removed from flow mould and flow inlets were punched.

A finished chip was bonded to a quartz slide with microfabricated Au electrodes. Prior to bonding the slides were sonicated in 2 % Hellmanex bath and rinsed thoroughly with tap water and ultra-pure DI-water. Oxygen plasma was applied to bond the PDMS chip irreversibly to the quartz substrate. The bonding process was finished by keeping the chip in 80 $°C$ oven at least for a night.

3.3.3 Electrode Alkylation

Alkylation was preformed to the Au electrodes of otherwise fully prepared microfluidic chip using method introduced elsewhere [65]. The chip was filled with 0.1 mM 1-Octanethiol solution (in ethanol) and allowed to flow through for 120 seconds, followed by flushing with ethanol. In order to have a thorough flush, 1 ml of pure ethanol was flown through the channel overnight. Any residual ethanol was evaporated in room temperature.

3.4 Amyloid Formation and Detection in a Chip

Two different approaches for amyloid formation were used: flow and incubation method. Both methods were conducted in a microfluidic chip and resulted in different kind of aggregates. Hence, different detection techniques were employed: fluorescence and impedance techniques. The steps for amyloid formation differed between flow (Fig. 21) and incubation method (Fig. 22). However, both methods began with SLB formation.

3.4.1 SLB Formation

Before starting all control valves of the chip were filled with DI-water and the function of valves were confirmed with microscope. When the valves needed to be closed, pressure of 1 bar was applied.

The SLB was formed by following the steps published elsewhere: [82, 83] with small changes. To start with, 100 μ M SUV solution was allowed to flow through the mf-chamber for 15 min keeping the peptide channel valve (valve 2) closed (Fig. 21 2.). This was followed by 1 h lipid incubation with peptide and outlet valves (valves 2 and 3) closed, consequently stopping the flow (Fig. 21 3.). During this hour the liposomes ruptured and formed the SLB on the quartz surface and hybrid bilayer on the alkylated gold electrodes.

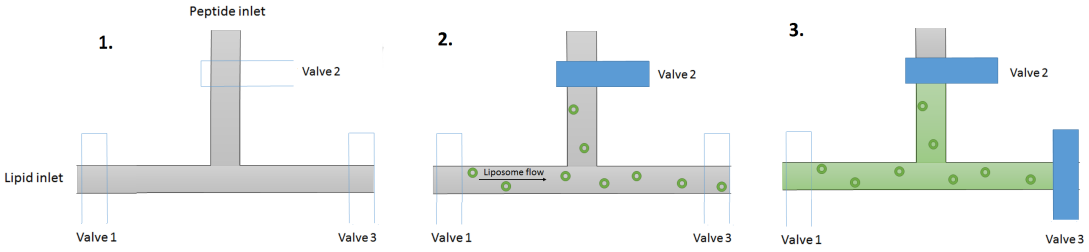

Figure 20: Steps for SLB formation in a microfluidic chip: 1) empty chip, 2) liposome flow, 3) lipid incubation.

The success of an SLB formation method was tested the before actual experiments with a lipid solution containing 2 per cent of fluorescent NBD-lipid. This lipid allowed a fluorescence recovery after photobleaching (FRAP) experiment to be conducted. In a FRAP experiment a small area of the SLB was illuminated with high intensity laser to photobleach the NBD molecules. If the bleached area retained it uniform fluorescence after few minutes, the surface must include SLB that enables the lateral diffusion of NBD molecules. This recovery was observed and the success of SLB formation was demonstrated.

After the formation of SLB the two methods differed.

3.4.2 Flow Method for Fluorescence Characterization

Method used for fluorescence characterization utilized a laminar flow typical to microfluidics and concentration gradient between peptide and lipid solutions to create continuous peptide aggregates. Like the name suggests, SLB formation was pursued by the flow of 40 μM liposome (in pH 4 buffer) and 0.4 μM peptide solution (in pH 7 buffer) keeping all valves open (Fig. 21 4.). This created a peptide/lipid and pH gradient focused in the centre of the channel. Thus, amyloid formation was triggered in this interface (Fig. 21 5.). Although the flow in mf-channel is laminar, diffusion causes mixing of the molecules between the different solutions. This was

seen especially in the end section of the channel where the formed aggregates were not as compact as in the entry section of the channel.

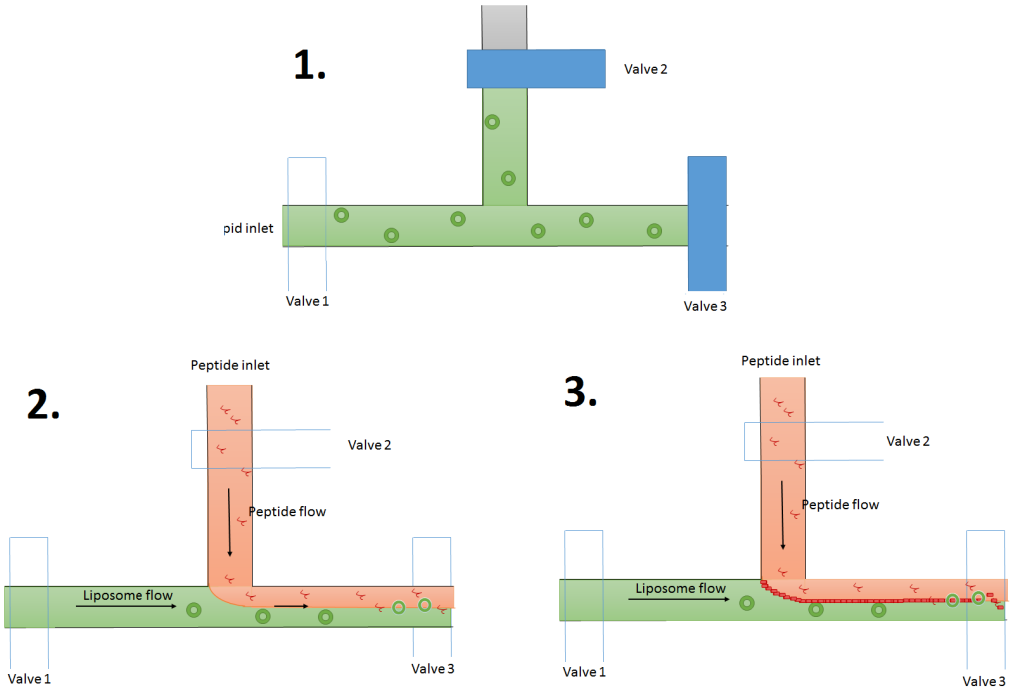

Figure 21: Steps of the flow method for amyloid formation: 1) prepared SLB, 2) simultaneous flow of lipid and peptide, 3) after hours or continuous flow a continuous peptide structure is formed to the interface of lipid and peptide flows

3.4.3 Incubation Method for Impedance Measurement

In the impedance measurement amyloids were formed with incubation method. This was necessary because the fluid flow has an evident effect in the measured impedance. In addition, flow can drive SLB out of the channel [83], which would have not been desirable.

To start with, an SLB was formed. This was followed by rinse of excess liposomes with buffer or ultra-pure DI-water (Fig. 21 2.). After the SLB formation and rinse the impedance measurements were started. Firstly, the organization of SLB in a constant AC voltage was measured. During the incubation flow was stopped by keeping valve 1 and 3 closed. However, valve 2 was let to be open to compensate the effect of vapour loss through the PDMS. Depending on the sample, measurement took from two to three days. This was followed by the recording of voltage and frequency characteristic curves. These curves were obtained by keeping either voltage or frequency constant and varying other as described in Section 3.2.2.

The SLB impedance measurements were followed by introduction of the peptide with a brief flow of peptide solution (Fig. 21 3.). The sample was again allowed to

incubate while keeping valves 1 and 3 closed, and valve 2 open. Hence, peptide inlet worked as a reservoir to fresh monomers and liquid. Similarly to SLB, conductivity was followed through the three day incubation, followed by the voltage and frequency characteristics measurements.

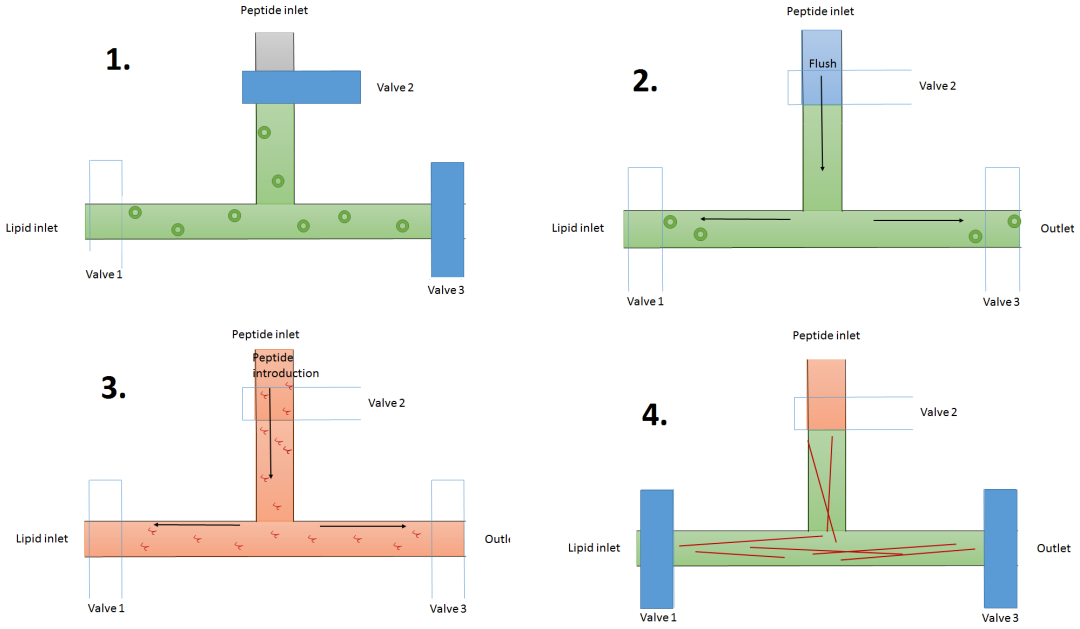

Figure 22: Steps of the incubation method for amyloid formation in a mf-chip: 1) SLB formation, 2) flush of the residual liposomes a with DI-water, 3) a brief flow of fresh peptide solution, 4) the fibrils were let to organize in stopped flow condition with valve 1 and 3 being closed. Impedance measurements were conducted between steps 2 and 3, during step 4) Electrodes are left out of the figure for clarity.

3.5 Fluorescence Spectroscopy

A fluorescence spectroscopy study was conducted to support the results made in microfluidic environment. Varian Eclipse fluorescent spectrometer was employed in titration and incubation study.

Experiments were performed in quartz cuvette with a constant magnetic stirring. Temperature was maintained in 25 $^{\circ}C$ with temperature control system. To start with, the emission and excitation spectrum of lipid solution were measured. This was followed by a titration of peptide solution into the lipid solution. The titration was performed by pipetting 2.5 μl aliquot and incubating the sample for 10 min. Incubation was followed by recording of emission spectrum with 345 nm excitation. This cycle was repeated until no change in the spectrum was observed. After titration the solution was let to incubate overnight. Next morning emission spectrum with different excitation wavelengths and excitation spectrum with different emission wavelengths were measured.

4 Results

Aforementioned materials and methods were employed to study amyloid formation. Both flow and incubation method gained encouraging novel results, which are exhibited in this section. In the first part amyloid aggregation in flow method was observed with bright field and fluorescence microscopy. In addition, fluorescence spectroscopy was applied to support the observations made in the microfluidic channel.

In the second part, the results from impedance measurements used with incubation method are presented. Firstly, results with different supported lipid bilayers are compared. This is followed by the data demonstrating the effect of amyloids to the SLB conductivity.

4.1 Fluid Flow Method/ Fluorescent Method

Novel observations from peptide organization in laminar flow with different lipid compositions and peptides were made. In addition, non-expected fluorescence with broad excitation and emission spectrum were imaged from the aggregates. These results are presented next.

4.1.1 Organization of Aggregates

To start with, different peptide and lipid concentration and compositions were used. When applying a relatively high concentration of peptide and lipid, an instant aggregation in the interface of 200 μM POPC:PPDPG (80:20 mol%:mol%) liposome and 12.3 μM KIGAKI peptide streams was detected (Fig. 23). After two hours of lipid/peptide flow, additional aggregation in the peptide side of the interface was observed. Hence, in order to have a more controlled and organized aggregation, the concentrations were decreased and different lipid compositions were used.

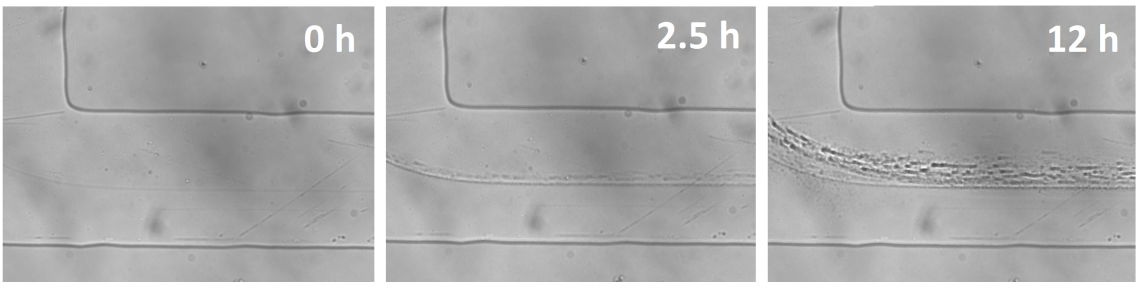

Figure 23: Aggregation of 12 μM KIGAKI peptide with 200 μM POPC:PPDPG (80:20) liposomes

An oxidized phospholipid, PazePC, was added to the liposomes, due to the proven enhancing effect of ox-pl in the induction of amyloid formation [94]. Under these

conditions the presence of 5 mol% of PazePC yield more ordered and interconnected aggregates (Fig. 24). Thus, aggregates of Aβ(1-42) and KIGAKI both without (Fig. 24 a and c) and with (Fig. 24 b and d) PazePC clearly differ upon microscopy. This could be due to the suggested ordering effect of ox-pl [5]. In the sample with KIGAKI and liposomes without PazePC multiple streams of aggregates are present compared to other samples. It seems that the interface of strands has shifted during the experiment. This can be due to the disturbance of aggregates to the laminar flow.

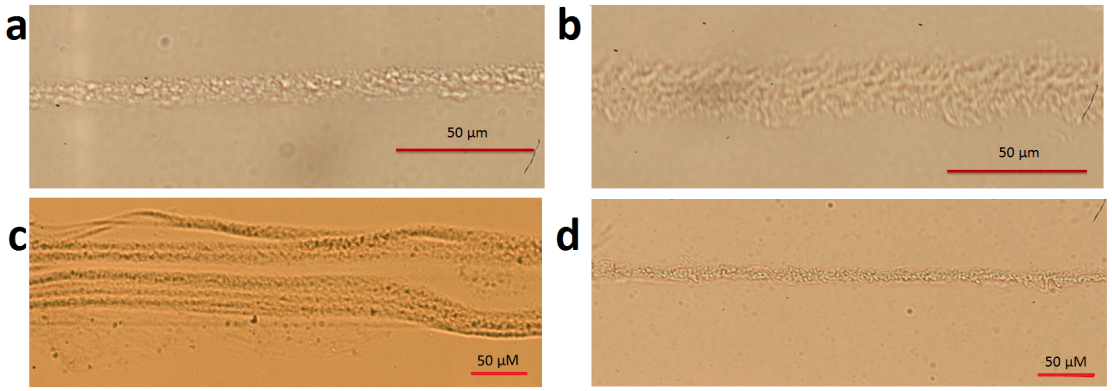

Figure 24: The effect of PazePC: a) Aβ(1-42) with liposomes without PazePC and b) with PazePC, and c) KIGAKI with liposomes without PazePC and d) with PazePC

4.1.2 Fluorescence of Aggregates

When examining the Aβ(1-42) samples under a fluorescent microscope, a bright emission was observed from both samples with all three filters (NBV, WIG and WIBA) (Fig. 25). The fluorescence was more intense for the highly interconnected aggregates in the presence of PazePC (Fig. 25 b), compared to the aggregates formed without PazePC (Fig. 25 a). Thus, suggesting more condensed packing and higher order of the aggregates. The intensity was even stronger after the sample was allowed to dry under ambient conditions, perhaps due to the concentration of the sample during the evaporation of excess water.

Similar behaviour was observed with KIGAKI peptide, which is reported to adopt β-sheet conformation [52]. The development of fluorescence intensity was monitored for two days. The fluorescence of the aggregates were observed before any aggregates were observed in bright field microscope (Fig. 26). The intensity increased with the aggregate growth. The highest intensity was observed with NBV filter, which has the lowest excitation and emission wavelengths. The signal observed through WIG filter, with the highest excitation wavelengths, had 5 times lower intensity compared to NBV. However, it was still four times higher than the signal from WIG filter, which is barely distinguishable from the image (Fig. 26). However, as mentioned in Section 3.2.1, the Hg lamp has different output intensities for the wavelength bands

of the used filters. Thus, because the intensity of the observed emission is correlated with the strength of the excitation light, no direct conclusion about the difference of intensity can be drawn. Instead, the changes in emission intensity should be considered.

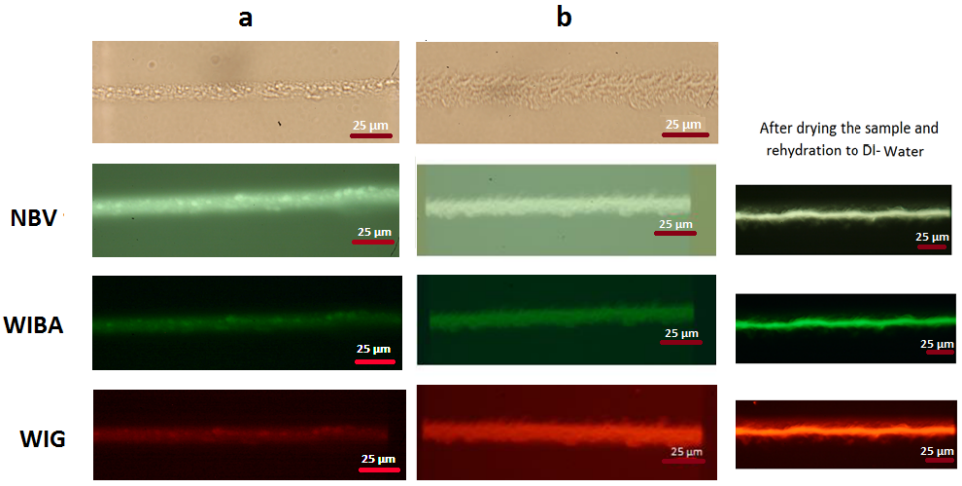

Figure 25: Aβ aggregates formed in the interface of liposome and peptide flow with a) POPC:PPDPG (80:20) and b) POPC:PPDPG:PazePC (75:20:5) liposomes. Images with bright field and three different fluorescence filters: NBV, WIBA and WIG.

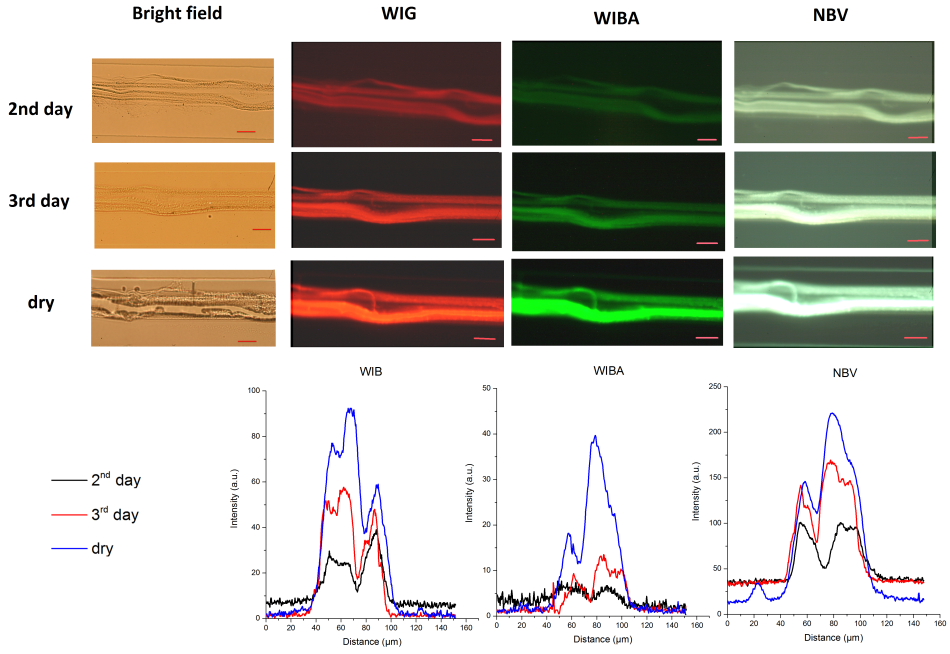

Figure 26: Aggregates formed from KIGAKI with POPC:PPDPG (80:20) liposomes after one and two days of the sample flow, and images of sample when it was let to dry for a night. In addition, intensity surface plots are shown for each fluorescent image. The red scales represent 50 μm.

After the second day, fluorescence emission intensity with all filters were considerably higher. Most efficient fluorescence was observed after the sample was allowed to dry. The most drastic rise of intensity was obtained with WIG filter. While the intensity at lower wavelengths just over doubled, fluorescence increased eight (WIG) and fivefold (WIBA) at the higher wavelengths, indicating changes in the organization of the aggregates when the sample became more concentrated.

This fluorescence resembles the intrinsic fluorescence of amyloids previously reported [7, 9–11]. However, the emission observed here is seen with excitation using visible region instead of UV-light. In addition, the emission seemed to have much broader spectrum. This would suggest stacking of pyrene moieties when PPDPG was interacting with amyloids. Thus, possibly creating trimers, tetramers etc. in the addition to monomers and excimers. In other words, this stacking could change the emission spectra of pyrene to higher wavelengths.

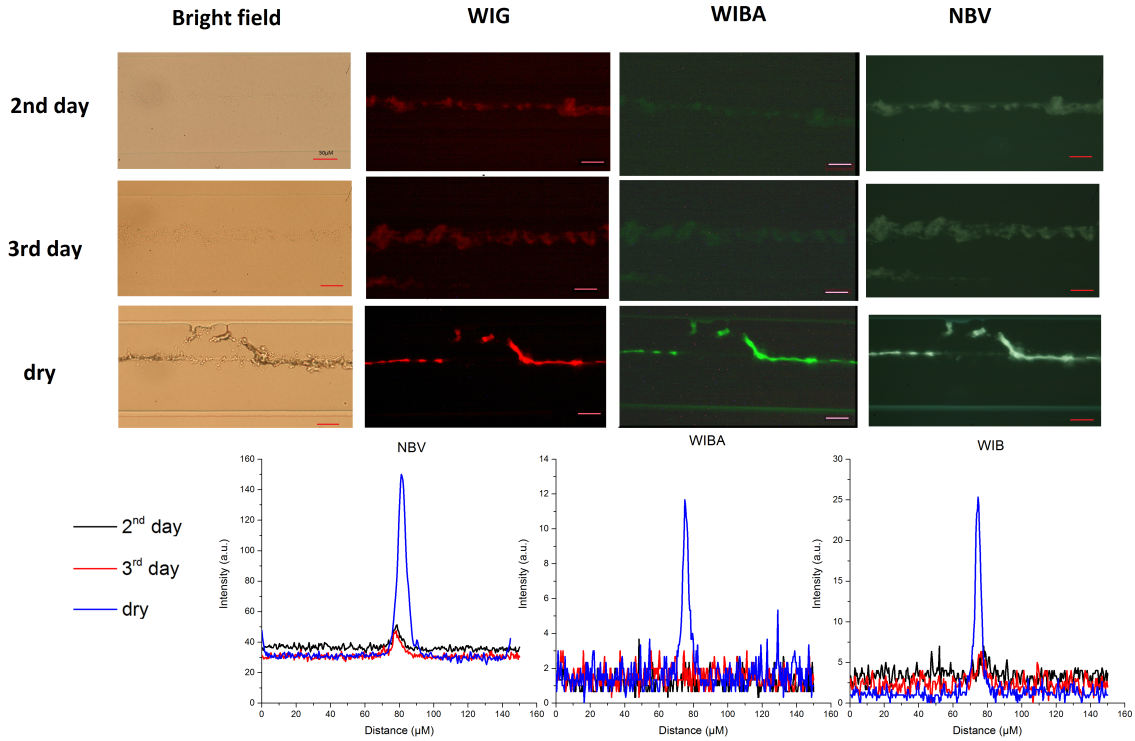

Figure 27: Aggregates formed from Aβ(1-42) with POPC:POPG:PazePC liposomes after one and two days of sample flow, and images of the sample when it was let to dry for a night. In addition, intensity surface plots are shown for each fluorescent image. The red scales represent 50 μm.

To test the hypothesis, the experiments were repeated using liposomes without pyrene-lapelled lipids. This resulted in considerably lower intensity of fluorescent emission (Fig. 27). However, some emission was once more observed with all three filters. The fluorescence with the two highest excitations and emissions were very weak and almost invisible before drying the sample.

These observations suggests that the aggregates formed without pyrene-lipid have an intrinsic emission spectrum similar to the aforementioned intrinsic fluorescence of amyloids [7,9–11]. However, when pyrene was present in the system, the fluorescence emission increased and the higher wavelengths got more pronounced. Thus, the pyrene moieties were responsible especially form the emission in higher wavelengths.

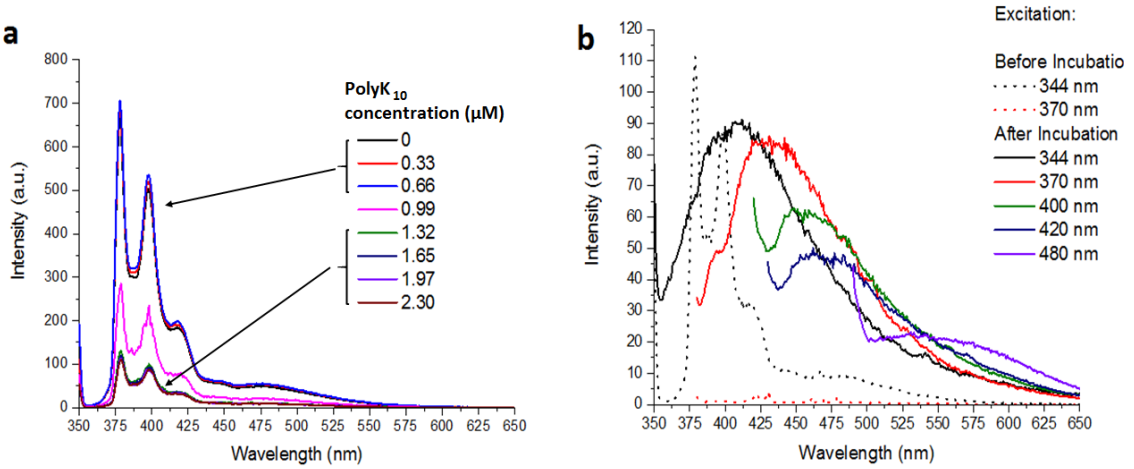

Figure 28: Change in a emission spectra during titration of 2.3 μM $PolyK_{10}$ into a 25 μM POPC:POPG:PPDPG (80:18:2) liposome solution (a) and after night of incubation (b).

Similar results were obtained with fluorescence spectroscope, when 25 μM liposome solution was incubated with 0.4 μM polyK$_{10}$ (Fig. 28). However, the observation of this effect seemed to be much harder with fluorescence spectrometer, in which the measurements were performed in 1.8 ml solution employing a cuvette. Hence, lacking the positive effects of small scale and high surface to volume ratio offered by the microfluidic chip. KIGAKI and Aβ peptides were experimented with, but only the purely cationic peptide polyK$_{10}$ was employed successfully.

The spectra changed two times during the experiment. The initial pyrene spectrum was almost entirely damped by the titration of the peptide (Fig. 28 a). However, after a 17 hour incubation the intensity was increased, and the shape of the spectrum was entirely changed (Fig. 28 b). The fine structure of pyrene spectrum disappeared and replaced by a wide peak centring at 420 nm with 344 nm excitation.

Similarly, the shape of excitation spectra changed. The sample emitted fluorescence with much higher excitation than pyrene usually does (Fig. 29). In other words, while no pyrene emission was seen with over 360 nm excitation wavelengths in the initial situation, after the incubation the sample could be excited with wavelengths over 450 nm (Fig. 28 b and 29). Furthermore, width of the excitation spectrum depended on the emission wavelength, contrary to initial situation, where only the intensity was changed (Fig. 29 dotted lines). This similar shift is apparent in in emission spectrum, where the peak is moved to higher wavelengths with higher excitations.

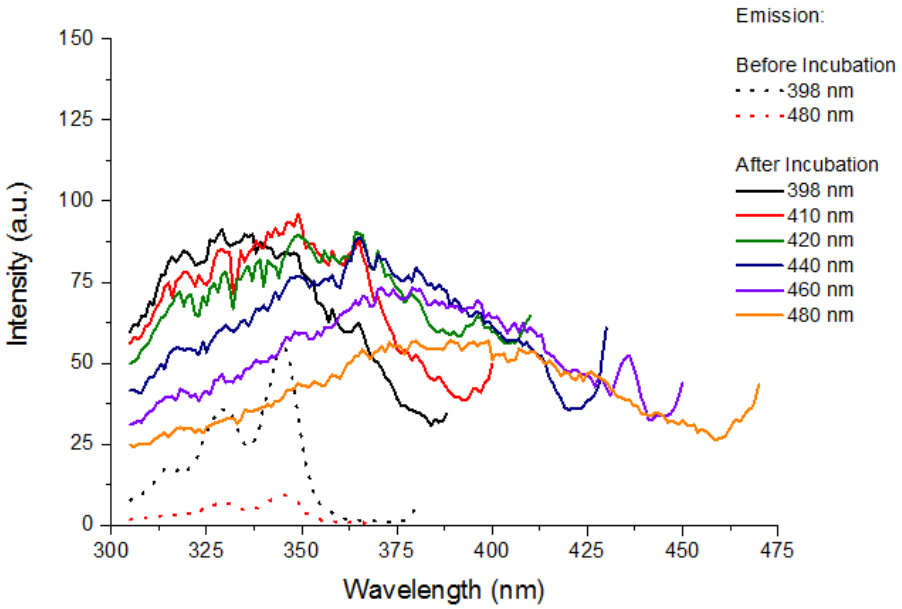

Figure 29: Change in an excitation spectra after titration of 2.3 μM $PolyK_{10}$into a 25 μM POPC:POPG:PPDPG (80:18:2) liposome solution. Dotted lines show the excitation spectrum just after the titration and full lines are excitation spectrum for different emission wavelengths after 17 h of incubation.

These observations support the fluorescence data obtained from the microfluidic chip. Thus, fluorescence shift to higher wavelengths in emission and excitation spectrum, and the disappearance of normal pyrene spectrum could suggest the formation of higher order pyrene stacks and interference of pyrene emission with the intrinsic fluorescence of the peptide aggregates.

4.2 SLB Method to Impedance Measurements

To examine the effect of amyloidogenic peptides in supported lipid bilayer, an incubation measurement from the organization of the sample was conducted. This was followed by the characterization of sample response to increasing input frequency and voltage. All SLBs were repeated in two different experiments. Each point in frequency and voltage characteristics measurements are an average from these two experiments. Similarly, the error bars for SLBs are the standard deviation of these two experiments. However, the peptide measurements were conducted only ones and the points are an average from three consecutive measurements from same sample. Standard deviation of these measurements is represented by error bars in peptide curves.

4.2.1 Impedance of SLB

To start with, different SLB compositions were measured in pH 7 buffer (Appendix A). In addition, chamber with pure buffer was measured as a reference. However, buffer showed a significant effect in the measurements. Hence, ultrapure DI-water was preferable option for impedance measurements.

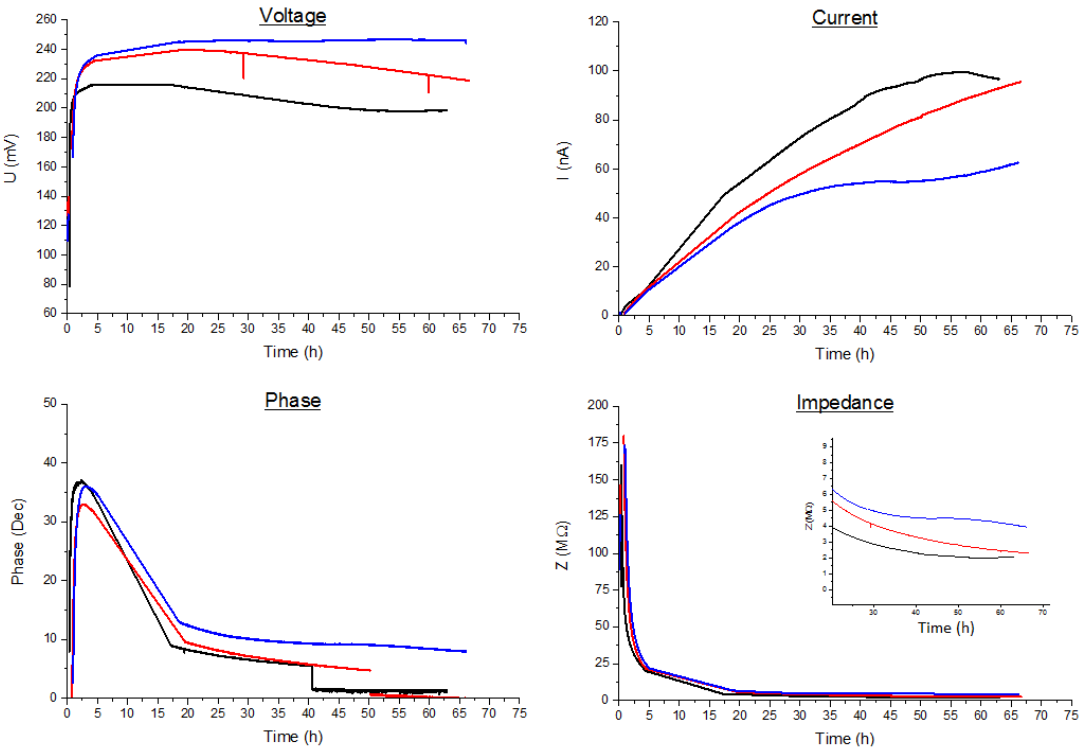

Figure 30: Conductivity data during incubation of POPC:PPDPG (—), PPDPC:PPDPG (—), and DMPC:DPMG (—) SLB with 1 V/ 777 Hz input voltage. PC:PG (mol%:mol%) relation was 80:20 in each SLB.

After the SLB was formed the experiment was started with a continuous measurement following the changes in the SLB conductivity during incubation (Fig. 30). First, it seemed that the SLBs were poorly conductive and almost no current passed the sample. Though, soon the current started to grow linearly. At the same time voltage increased rapidly and reached its plateau for PPDPC:PPDPG SLB in 240 mV. However, POPC:PPDPG SLB showed a small drop in voltage before finding a plateau at 200 mV and for DMPC:DMPG SLB voltage decreased through the whole experiment reaching 220 mV when the measurement was ended. Contrary to voltage, current had more modest growth rate. POPC:PPDPG SLB reached the highest current value (97 nA) and DMPC:DMPG SLB the lowest (60 nA). Similarly to voltage behaviour, current curve of PPDPC:PPDPG SLB did not reach the plateau before measurement was ended. These results suggest that the organization of DMPC:DMPG SLB in AC field is much more rapid than the SLBs containing bulky

pyrene-lipid moieties (PPDPC and PPDPG). Hence, PPDPC:PPDPG consisting purely from pyrene-lipids seemed to have the slowest organization. The phase of the measured signal was highly positive at the beginning of incubation, peaking at 30-40 decrees. However, a big drop between 5 to 19 h is due to saturation of current signal and the change of a resistor in pre-amplification circuit. This correlation between the resistor value and phase complicate the interpretation of the phase data.

Impedance for each sample showed an exponential decrease from near 175 MΩ to approximately 2 MΩ for POPC:PPDPG, 2.5 MΩ for PPDPC:PPDPG and 4 MΩ for DMPC:DMPG consequently. Although DMPC:DMPG showed the most rapid organization, the impedance results suggests that it is the worst electric conductor.

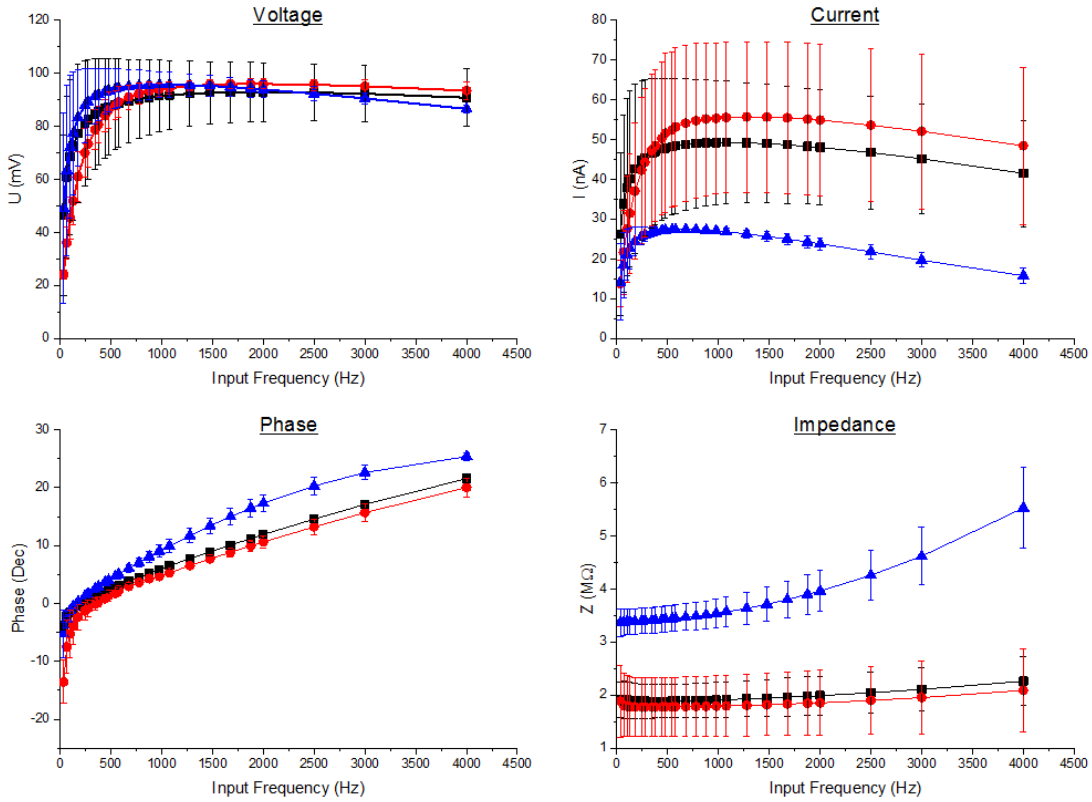

Figure 31: Frequency characteristics of POPC:PPDPG (■), PPDC:PPDPG (●), and DMPC:DPMC (▲) SLB using 0.4 V as input voltage. PC:PG (mol%:mol%) relation was 80:20 in each SLB.

Similarly, DMPC:DMPG had much higher impedance throughout the frequency spectrum (Fig. 31) compared to the SLBs containing pyrene-labelled lipids. In addition, it showed a higher dependence in the applied frequency. This is seen in voltage, current, and impedance graphs. In the first two DMPC:DMPG peaks at the low frequencies followed by steady decrease of voltage and current signal. For POPC:PPDPG and PPDPC:PPDPG SLBs voltage signal has a minimal decrease in higher frequencies. However, current signal is more affected by the frequency of the applied signal.

For all SLBs the phase increases from negative in low frequencies to positive in higher frequencies, thus meaning growth of the inductive component of the system. The change in real and imaginary parts of impedance is illustrated in Cartesian coordinates (Fig. 32). For pyrene moieties containing SLBs had relatively stable real part thus resistance near 2.25 MΩ, but the reactance varies from -0.5 MΩ for 33 Hz input to 1 MΩ for 4000 H. DMPC:DMPG SLB had much higher resistance part. In addition, it increased from 3.5 to nearly 5.5 MΩ with growing frequency. At same time the reactance change from -0.25M Ω to little over 2.5 Ω.

Interestingly, the error bars shoving standard deviation between two measurements are considerably wide for POPC:PPDPG, PPDPC:PPDPG (Fig. 31). This is most apparent in the current graph and with PPDPC:PPDPG. Contrary, the phase shows almost no variation between the two measurements. This phenomena, might be due to the slower organization of pyrene lipid containing SLB, since DMPC:DMPG SLB shows really low deviation in current measurements.

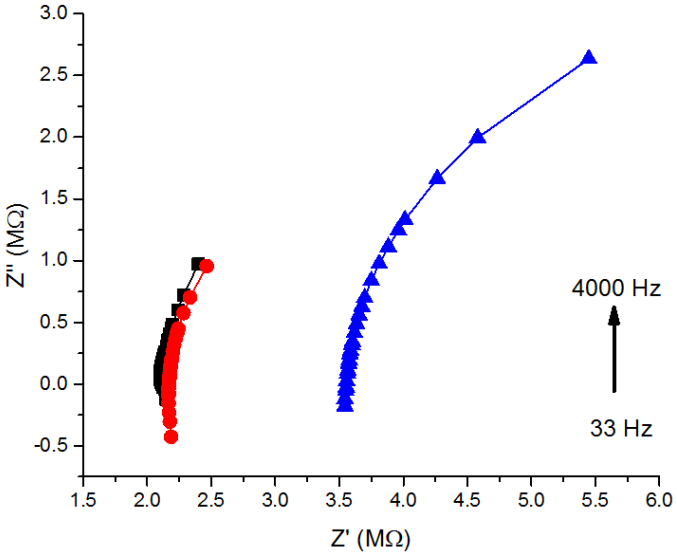

Figure 32: Impedance in Cartesian coordinates, where POPC:PPDPG (■), PPDC:PPDPG (●), and DMPC:DPMC (▲) 0.4 V as input voltage. PC:PG (mol%:mol%) relation was 80:20 in each SLB.

Aforementioned trends are also recognized in voltage–characteristics measurements (Fig. 33). Hence, DMPC:DMPG SLB has the highest voltage and lowest current with all input voltages. All samples had linearly growing response to increasing voltage, thus no change in impedance was observed. With low input voltages phase was negative in all samples. After 0.5 V all samples found a plateau. The sudden decrease in both pyrene-SLB samples is due to resistor change in pre-amplification circuit.

These results served as a reference to the experiments with amyloidogenic peptides. The POPC:PPDPG SLB was chosen to be used in the following experiments due to its low impedance and relatively low amount of expensive pyrene-labelled lipid .

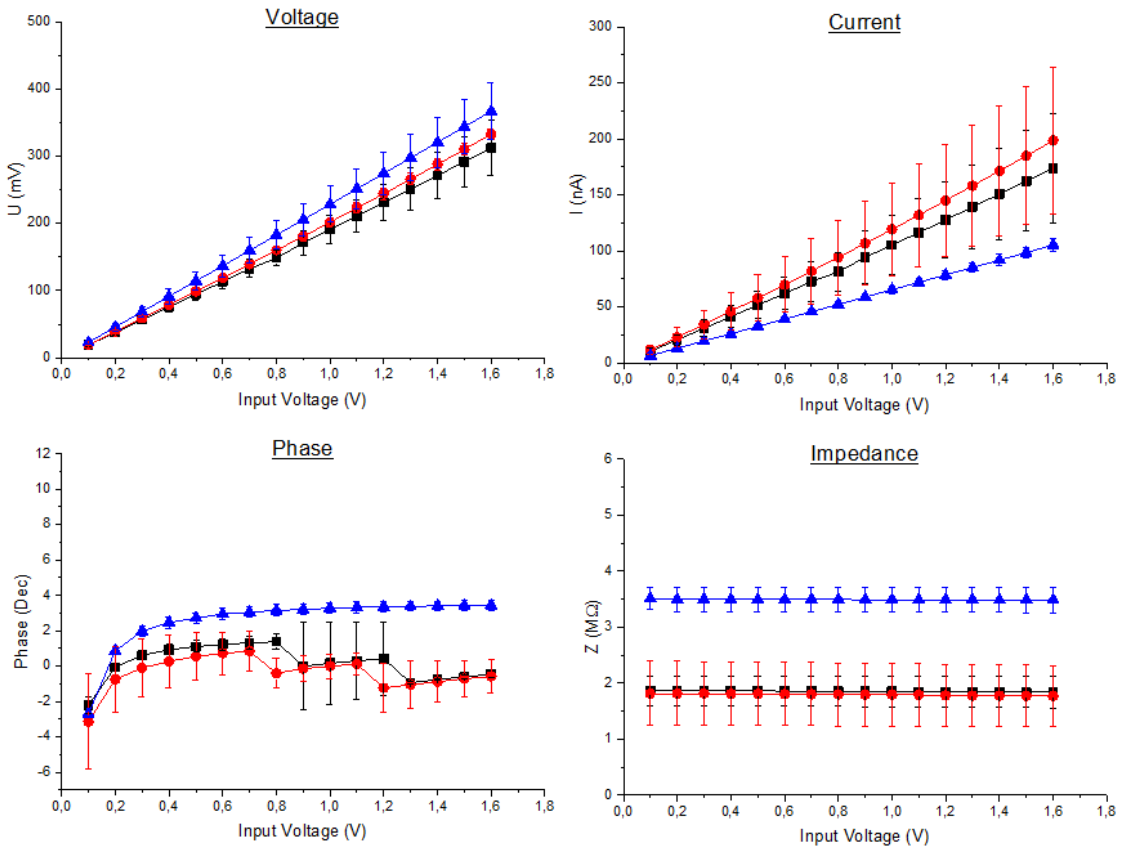

Figure 33: Voltage characteristics of POPC:PPDPG (■), PPDC:PPDPG (●), and DMPC:DPMC (▲) SLB using 344 Hz as input frequency.

4.2.2 The Effect of Peptide

After all measurements with SLB, peptide solution (TempB or KIGAKI) was added on the bilayer. Due to the disturbance of fluid flow and introduction of the peptide to the system, organization of the SLB was lost and sample was again poorly conductive in the beginning of the experiment.

Similarly to pure POPC:PPDPG SLB, voltage experienced a quick increase in the beginning of the incubation (Fig. 34). However, this occurred later with peptide samples than with pure SLB alone. Although the voltages of 210 mV with TempB, and 250 mV with KIGAKI where only a modest increase from the 200 mV for pure POPC:PPDPG SLB, the currents differed dramatically. The increase of current during the measurement was remarkably slower for SLB with a peptide. Hence, the SLB with TempB reached only to 21 nA and the SLB with KIGAKI to 35 nA, compared to 97 nA for the pure POPC:PPDPG SLB. These resulted about three (KIGAKI) and four times (TempB) higher impedances for.

The results suggest that both peptides disturb the organization of the SLB. KIGAKI having higher percentage of cationic amino acids, was expected to interact more

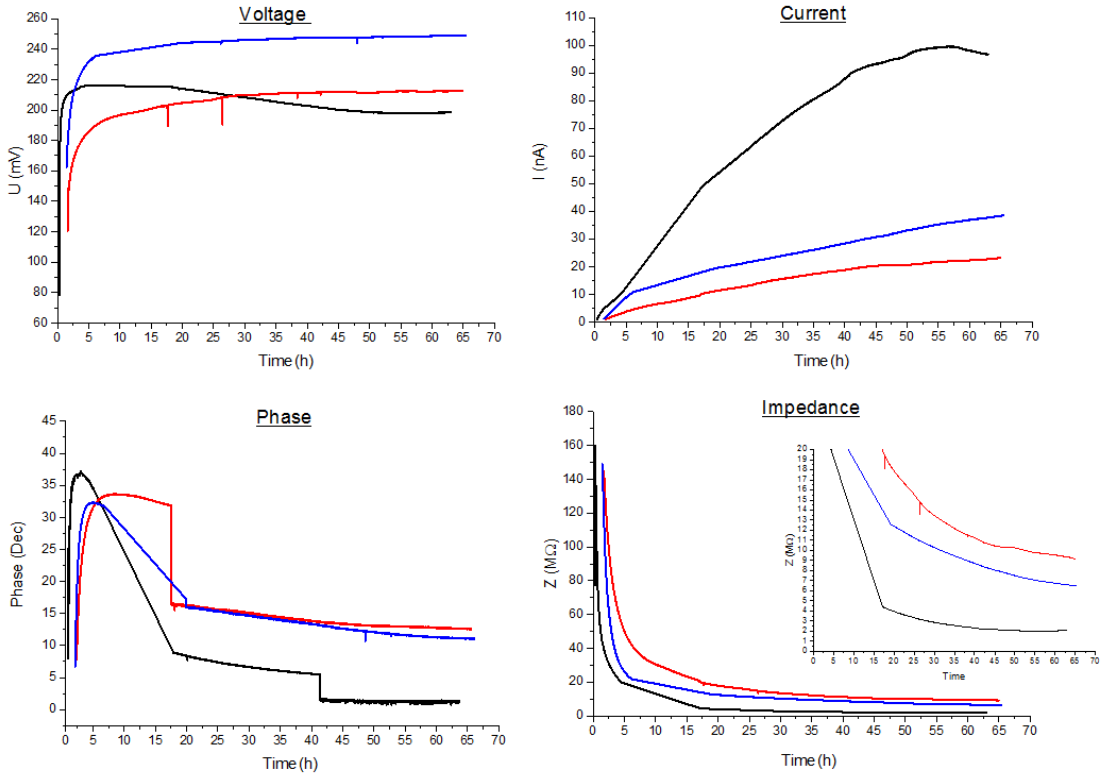

Figure 34: Conductivity data during incubation of POPC:PPDPG (80:20 mol%:mol%) SLB (—), SLB with 0.4 μM TempB (—), and SLB with 0.4 μM KIGAKI (—) peptide with 1 V/ 777 Hz input voltage. PC:PG (mol%:mol%) relation was 80:20 in each SLB.

strongly with the acidic PPDPG. However, it did not have as radical effect as TempB had to the POPC:PPDPG SLB. Because the effect of AC electric field to these peptide is not understood, it is impossible to know, where these differences could stem from.

The lower conductivity affected considerably to frequency characteristics measurements (Fig. 35). This is seen in loss of data from higher frequencies in measurements taken from the SLB with peptide due to decay of signal quality in nA currents. In order to detect these signal, additional amplification to the signal would have been needed.

Although all frequencies could not be measured, important trends can be seen. Hence, SLBs after the peptide addition are more sensitive to frequency changes. The POPC:PPDPG SLB had a big difference in voltage and current values between two measurements. However, this deviation is not significant when impedances are compared. While POPC:PPDPG impedance is near 2 MΩ trough the frequency spectrum (33 to 4000 Hz), SLB with KIGAKI had roughly three times higher frequency at low frequencies increasing to 11 MΩ at 3000 Hz input frequency. This was the last point that could be measured. TempB showed little under 8 MΩ

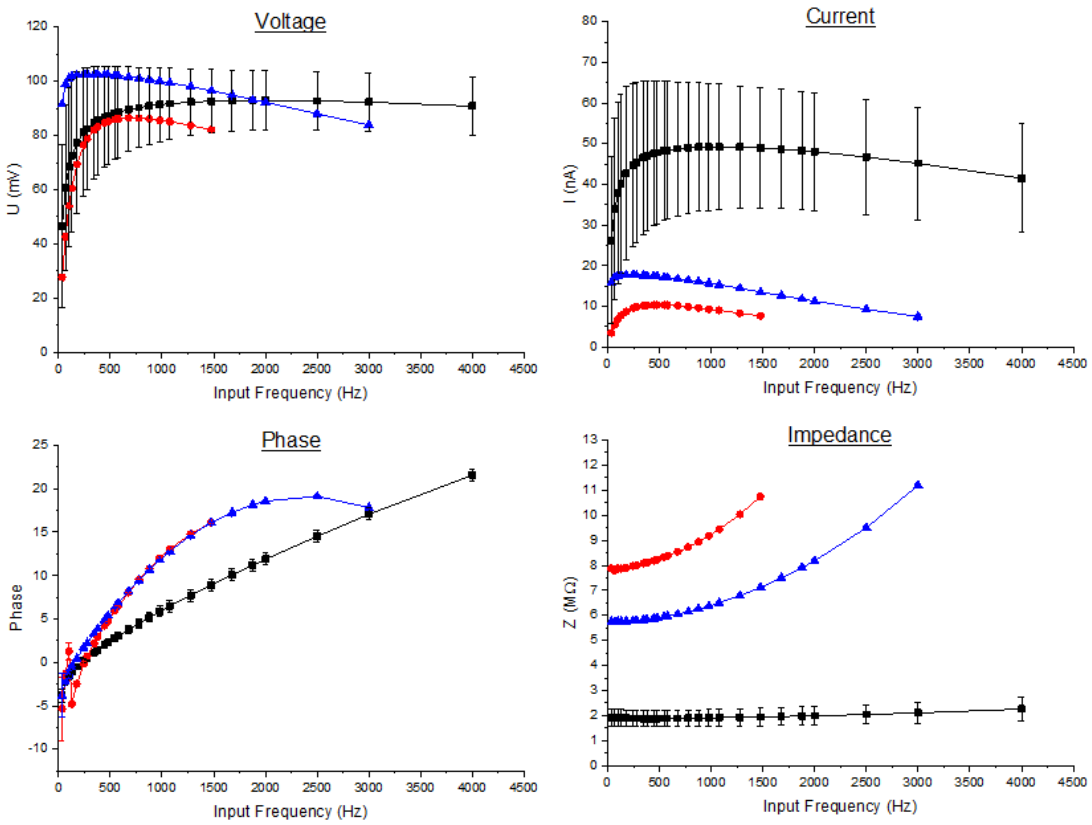

Figure 35: Frequency characteristics of POPC:PPDPG (80:20 mol%:mol%) SLB (■), SLB with 0.4 μM TempB (●), and SLB with 0.4 μM KIGAKI (▲) peptide using 0.4 V as an input voltage. SLB curve is an average from two separate experiments and the error bars are standard deviation from each point.

impedance at 33 Hz and reached the limit of 11 MΩ at just before 1500 Hz.

Both peptides had similar effect to the measured phase. Although, less measurement points were acquired with TempB sample, the points follow almost identically to the trend of KIGAKI sample. Only the few first points have some deviation mostly due to the pour signal at first measured frequencies. As seen in the incubation measurement (Fig. 34) the addition of peptide increased the reactance component of the sample. However, the phase for sample containing KIGAKI started to decrease in highest frequency.

From the Cartesian coordinates (Fig. 36) can be seen, how the quality of impedance changed. If the KIGAKI and TempB curves are extrapolated few frequencies further, the curves would most definitely cross each other. Meaning there must be some difference in the conduction method and the organization of SLB/peptide systems.

The voltage characteristics followed the same trends that were observed with incubation and frequency characteristics measurements (Fig 37). The peptide samples could not be measured with the lowest voltages due to low signal. SLB with TempB had

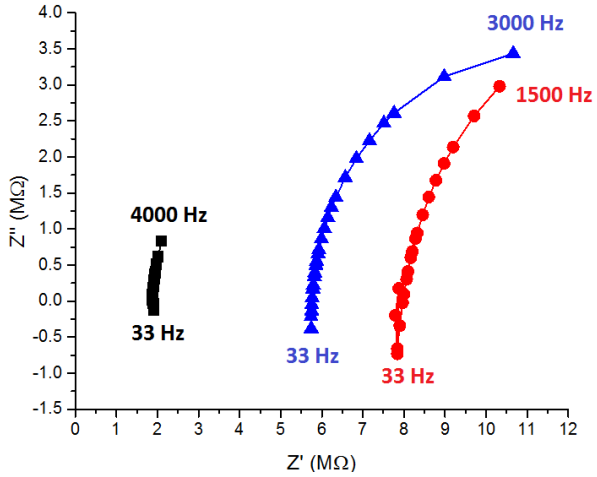

Figure 36: Impedance in Cartesian coordinates, where POPC:PPDPG (80:20 mol%:mol%) SLB (■), SLB with 0.4 μM TempB (●), and SLB with 0.4 μM KIGAKI (▲) peptide using 0.4 v as input voltage.

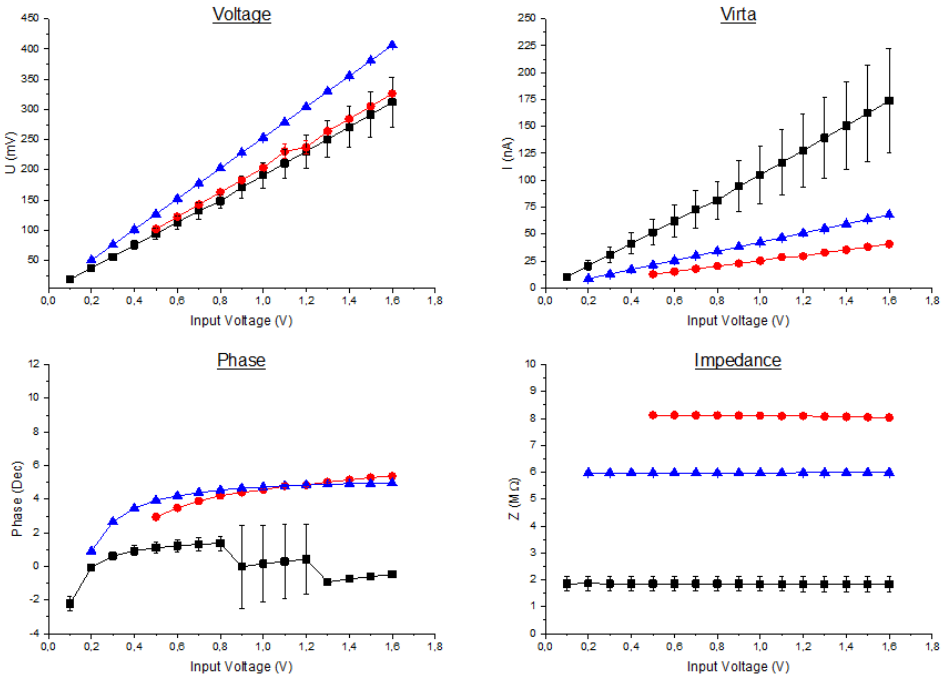

Figure 37: Voltage characteristics of POPC:PPDPG (80:20 mol%:mol%) SLB (■), SLB with 0.4 μM TempB (●), and SLB with 0.4 μM KIGAKI (▲) peptide 344 Hz as input frequency.

similar response to the varied voltage than the pure POPC:PPDPG SLB. However, SLB with KIGAKI had higher voltage and steeper response. However, what comes to current, the input voltage increase did not have as much effect to the samples with peptide as the pure SLB. Since both voltage and current grew linearly when

input voltage was increased, the impedance was constant trough the experiment staying approximately at 2 MΩ, 6 MΩ, and 8 MΩ for POPC:PPDPG SLB, SLB with KIGAKI, and SLB with TempB consequently. The phase showed again shift to positive decrees after addition of peptide, and both peptides seemed to have quite similar effect to the SLB phase.

These results show a clear change in the conductivity of the POPC:PPDPG SLB after peptide was added to the system. Especially the current was highly decreased. In addition, both voltage and current became more sensitive to the applied frequency. This indicates that similar systems could be used to characterize lipid bilayer fluidity and lipid-peptide interactions. However, more experiments must be conducted to understand the system more thoroughly. This is discussed more in next Section.

5 Discussion

Chapter 4 presented the results related to amyloid formation and observation in a microfluidic chip. This section discusses how well the results meet the aims of the study. Furthermore, the reliability of the flow and incubation methods and results are evaluated and possible future studies suggested.

The flow method resulted in relatively big aggregates with multiple different morphologies in the interface of adjacent peptide and liposome flows (Fig. 24). This observation clearly indicates that some organizing interaction occurred in this interface. In addition, the high-intensity fluorescence with and without pyrene lipids suggests that the aggregates had highly ordered and compact nano-structures. As discussed earlier, the fluorescence emission was observed with all filters and different excitation and emission wavelengths (Table 1). This suggests that aggregates have a broad emission spectrum. However, due to the aforementioned properties of Hg lamp (Fig. 14), no direct conclusions can be drawn from the obtained intensity plots.

The fluorescence seemed to be stemmed from pure peptide when organized to a concentrated aggregate and from pyrenes interacting with peptides and adjacent pyrene molecules. Although, additional support for these observations were obtained from a fluorescence spectroscopy experiment (Fig. 28 and 29), due to difference in the environment in bulk and Mf studies, no straight connection to these studies can be claimed.

The aforementioned concerns could have been avoided, if the fluorescence spectrum had been obtained straight from the microfluidic channel. In fact, an attempt to record an emission spectrum with a fluorescence spectrometer connected to a inverted microscope was performed. By this system samples in microscope stage could be measured. However, it seemed that due to the damping of excitation intensity when travelling through optical fibre connecting the spectrometer and microscope, no emission was observed. Hence, the small sample size (nanoliters) would have required high excitation intensity and/or more sensitive detector.

The PDMS chip limits the experiments that can be conducted to the sample. Similarly to the acquisition of an emission spectrum, custom systems need to be engineered if additional information from the mf-system is desired. This is mainly due to the fact that the grown aggregates cannot be removed from the chip. For example, experiments to obtain information from a secondary structure to confirm the β-sheet rich content characteristic to amyloid fibrils would have been natural continuum to these experiments. Fourier transform infrared spectroscopy (FTIR) is conventionally used for this purpose [95]. However, customizing a FTIR instrument to measure data from a microfluidic chip was not possible in the scope of this thesis. Further, electron microscopic methods that would have elucidated the nano-structure of the aggregates were not possible either.

There are multiple different additional experiments that would have been interesting to perform on the aggregates formed with the flow method. However, the method is

quite simple and the interaction with lipids is evident, due to the highly fluorescent aggregates formed.

Compared to flow method, the incubation method has more uncertainty. Firstly, the success of alkylation could not be confirmed with AFM. Secondly, the SLB formation was only verified in initial experiments with a fluorescent lipid NBD in fluorescence recovery after photobleaching (FRAP) tests. Thirdly, the effect of applied electric field to the SLB is has not been studied. For example, a low frequency AC voltage has been used to create giant unilamellar vesicles [96] demonstrating that AC fields have an effect on organization of phospholipids in bilayer. However, the impedances measured in this thesis suggest that there must be a well-organized conductive structure between the electrodes. This indicates the success of SLB formation and organizing effect of the electric field.

As far as I know, no comparable measurements from lipid bilayers with surface electrodes have been published. The most relevant study was conducted with SLB formed on mica and the conductivity was measured with scanning tunneling microscopy (STM) [97]. The SLB measured consisted from fully saturated phospholipids (DPPC and DPPE), and only pA currents were recorded compared to 1000 times higher currents measured in this thesis. It was suggested that the conductivity of DPPC/DPPE bilayers is due to the dense network of water molecules on the SLB surface.

However, different phospholipids were used in this work. Thus, in addition to the network of adsorbed water molecules the SLBs employed in this thesis might possess different conductivity mechanisms. For example, the acidic phospholipids might serve as proton carriers and enhance the conductivity. Further, it has been suggested that the double bonds in un-saturated phospholipids, such as POPC, might create a conductive molecular orbital, if properly arranged [98]. Hence, this supports the results with different SLBs (POPC:PPDG, PPDPC:PPDPG, and DMPC:DMPC). The lowest conductivity was observed with DMPC:DPMG SLB that lacks the double bond network (Fig.30, 31, 32, and 31).

The addition of amyloidogenic peptide seemed to disturb the conduction methods (Fig. 34, 35, 36, and 37). It could be due to the high affinity of cationic peptide towards the acidic lipids (PPDPG) containing SLB, thus disturbing the network of adsorbed water molecules (Fig. 38 2.). The conformational changes in adsorbed peptides might also rearrange the SLB, affecting the network of double bonds buried into the SLB, by creating PPDPG barriers (Fig. 38 3.). Further, it is known that amyloids can extract membrane lipids [49, 50] and this can also affect to the conductivity of SLB.

However, also a thin water layer between the SLB and quartz substrate could contribute to the conductivity. This 'buried' side of the SLB cannot be affected by peptides, unless they can travel through the hydrophobic interior of the SLB.

In addition to the measured PC/PG SLBs, an experiment with pure PC bilayer would have been interesting to conduct. This would have served as a reference

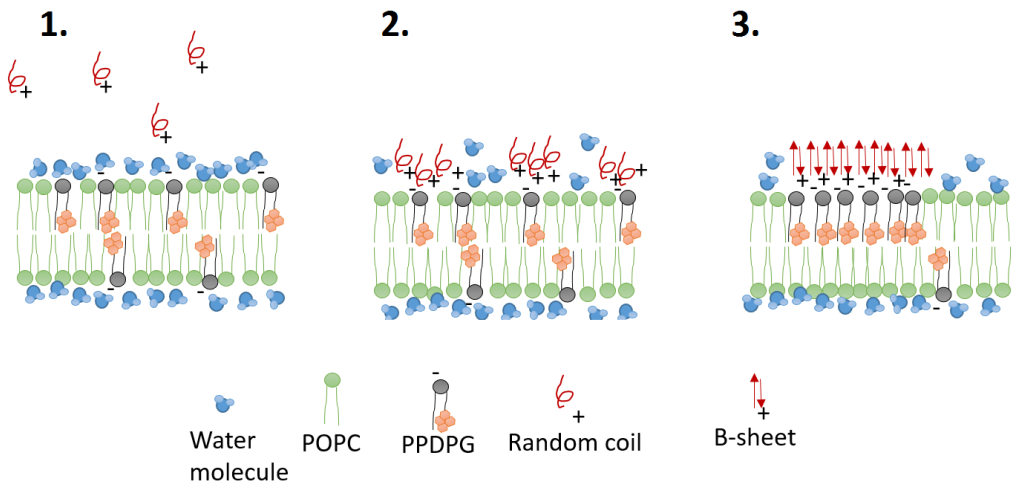

Figure 38: Simplified presentation of the suggested lipid-protein interaction. 1. Unfolded peptide (random coil) is introduced on the bilayer by peptide solution flow. 2. The local concentration of the peptide is growing near the negative PPDPG lipids, disturbing the network of adsorbed water molecules. 3. These positive peptides attract even more PPDPG lipids to proximity and the peptide starts to fold itself into β-sheet structure.

to the interaction of peptides with acidic PG lipids. For example, if the PC SLB conductivity would not have been affected by the peptide as much as PC:PG SLBs, the role of PG/peptide-interaction could have been confirmed. However, the major disadvantage of the used system was the measurement time. Experiment with one SLB and peptide type took up to 6 day, with a single experiment been performed.

This problem can be tackled with two different approaches: reducing the measurement time, or enabling the measurement of multiple samples. The former might be possible by changing the electrode design: by bringing the electrodes closer, the area of measured bilayer would decrease. Hence, the organization time of the SLB between the electrodes would increase and the incubation time could be decreased from three days. The latter would either require building another set-up, or redesigning the Mf-chip. The first solution is expensive and space consuming. However, the second option is more feasible. A chip with multiple isolated channels, common signal feed electrodes, and individual measurement electrodes would work. In addition, a suitable pre-amplification circuit and the LabVIEW program to alternately measure the signal from different electrodes would be needed.

In addition to the aforementioned studies with DMPC SLB, the effect of cholesterol to the lateral conductivity would be interesting to see due to its known property of inducing phase separation of phospholipids [99]. Further, the result with amyloidogenic peptides with high β-sheet content should be compared to results from peptides with more diverse secondary and aggregation structures to further characterize the system. Moreover, multiple different peptide concentrations would be interesting

to employ to see if the aggregates' sizes play a role in the conductivity. Hence, if a continuous network of amyloids could be created between the electrodes, maybe the conductivity of the continuous network would bring an additional enhancing component to the conduction system.

To further analyse the nature of the conductivity, an equivalent circuit should be constructed. Although this work does not include one, simplified guesses of the equivalent circuit can be made (Fig. 39). It is known that the alkylation brings a capacitive (Fig. 39 C_{thiol}) and a resistive (Fig. 39 R_{thiol}) component to the contact between the electrodes (Fig. 39 e1, e2, e3, and e4) and the sample (Fig. 39 Z_1, Z_2, and Z_3) [100]. Thus, this interface is usually modelled with a simple RC-circuit. When it comes to the sample composed from an SLB or an SLB and a peptide, the situation is more complicated. Without computational methods, and the help of a sophisticated computer program, all that can be said is that the sample consist from impedance elements. These elements include capacitive, resistive, and inductive components. When interpreting the Cartesian plots (Fig. 32 and 36), it seems that the resistive part is dominant. In addition, a considerable inductive part is seen, but in the smallest frequencies the capacitive part is dominant over inductive. However, the quality of connections (parallel or series) cannot be reasoned.

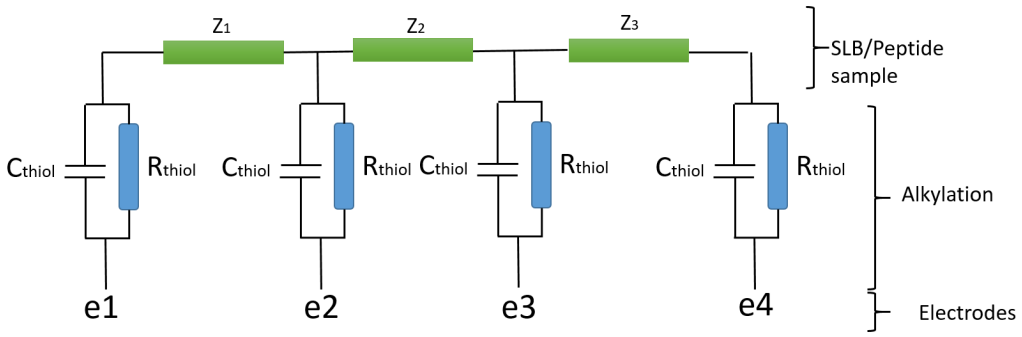

Figure 39: A simplified model of the possible equivalent circuit. The 1-octanethiol monolayer (C_{thiol} and R_{thiol}) connecting the electrodes (e1–e3) to the sample (Z1–Z3).

As stated in the introduction, the aim of this thesis was to find novel approaches to characterize the formation of amyloid fibres in a microfluidic system. The results presented here (Section 4) manifest that both methods might provide possibilities in amyloid research. Both methods can be used as a label free techniques excluding the possibly result corrupting effects of amyloid specific dyes. However, as mentioned above, more experiments are needed to characterize the methods.

6 Conclusions

This thesis investigated novel characterization methods for the amyloid fibril growth. A microfluidic approach was chosen to serve as the platform for the experiments. This allowed the miniaturization and customization of experiment environment, thus a microfluidic channel with flow control was prepared. In addition, microfabricated surface electrodes were added to allow the performance of impedance spectroscopy measurements.

Two different approach for amyloid formation were used: flow method and incubation method. The former showed how amyloidogenic peptides aggregate in the interface of peptide and lipid solution streams in a microfluidic environment. Aggregation was triggered by the concentration gradient of lipid and peptide between the laminar streams. In addition, the lipid composition seemed to play a role in the organization of the peptide aggregates. Thus, the presence of an oxidized phospholipid, PazePC, in the system resulted in more ordered aggregates. Another finding was, that despite the absence of traditional amyloid specific dyes, a strong fluorescence of the aggregates upon excitation with visible light wavelengths was observed. This fluorescence was considerably amplified in two cases: 1) when aggregates were more organized and interconnected and 2) in the presence of pyrene-labelled lipids. The former can result from be because of the more dense packing of peptide in more organized aggregates. The latter indicates an interaction between pyrene-labelled lipids and amyloids and possible stacking of the pyrene moieties.

The second method involved electrical impedance measurements with surface electrodes. Up to 200 nA currents were measured with from PC/PG SLB resulting impedance little under 2 MΩ. These were measured from SLB containing purely pyrene lipids. Lowest conductivity was recorded with DMPC:DMPG. Comparing these results with previously published data with PC/PE SLBs the much higher current observed here, suggests that lipids used in this thesis possess different conduction mechanisms.

This SLB conductivity was disturbed by the addition of amyloidogenic peptides by considerably increasing the inductive and resistive part of impedance. Hence, it was evident that the peptides were interacting with SLB and affecting its conductive properties. These results suggests that similar methods could be used as amyloid sensors. However, additional engineering to the system would be needed to decrease the measurement time and allow multiple samples to be analysed simultaneously.

Both methods showed results that provide novel information from formation amyloids and could serve as possible characterization approaches for amyloid research. However, additional reference experiments with different peptides and verification of peptide nano-structure would be the next step to confirm our observations so far.

References

[1] F. Chiti and C. M. Dobson, "Protein misfolding, functional amyloid, and human disease," *Annu. Rev. Biochem.*, vol. 75, pp. 333–366, 2006.

[2] M. Zhu, J. Li, and A. L. Fink, "The association of α-synuclein with membranes affects bilayer structure, stability, and fibril formation," *Journal of Biological Chemistry*, vol. 278, no. 41, pp. 40186–40197, 2003.

[3] M. Bokvist, F. Lindström, A. Watts, and G. Gröbner, "Two types of alzheimer's β-amyloid (1–40) peptide membrane interactions: aggregation preventing transmembrane anchoring versus accelerated surface fibril formation," *Journal of molecular biology*, vol. 335, no. 4, pp. 1039–1049, 2004.

[4] J. D. Knight and A. D. Miranker, "Phospholipid catalysis of diabetic amyloid assembly," *Journal of molecular biology*, vol. 341, no. 5, pp. 1175–1187, 2004.

[5] A. K. Mahalka, C. P. J. Maury, and P. K. Kinnunen, "1-palmitoyl-2-(9'-oxononanoyl)-sn-glycero-3-phosphocholine, an oxidized phospholipid, accelerates finnish type familial gelsolin amyloidosis in vitro," *Biochemistry*, vol. 50, no. 22, pp. 4877–4889, 2011.

[6] C. Aisenbrey, T. Borowik, R. Byström, M. Bokvist, F. Lindström, H. Misiak, M.-A. Sani, and G. Gröbner, "How is protein aggregation in amyloidogenic diseases modulated by biological membranes?," *European Biophysics Journal*, vol. 37, no. 3, pp. 247–255, 2008.

[7] L. L. del Mercato, P. P. Pompa, G. Maruccio, A. Della Torre, S. Sabella, A. M. Tamburro, R. Cingolani, and R. Rinaldi, "Charge transport and intrinsic fluorescence in amyloid-like fibrils," *Proceedings of the National Academy of Sciences*, vol. 104, no. 46, pp. 18019–18024, 2007.

[8] T. Scheibel, R. Parthasarathy, G. Sawicki, X.-M. Lin, H. Jaeger, and S. L. Lindquist, "Conducting nanowires built by controlled self-assembly of amyloid fibers and selective metal deposition," *Proceedings of the National Academy of Sciences*, vol. 100, no. 8, pp. 4527–4532, 2003.

[9] A. Shukla, S. Mukherjee, S. Sharma, V. Agrawal, K. R. Kishan, and P. Guptasarma, "A novel uv laser-induced visible blue radiation from protein crystals and aggregates: scattering artifacts or fluorescence transitions of peptide electrons delocalized through hydrogen bonding?," *Archives of biochemistry and biophysics*, vol. 428, no. 2, pp. 144–153, 2004.

[10] S. Sharpe, K. Simonetti, J. Yau, and P. Walsh, "Solid-state nmr characterization of autofluorescent fibrils formed by the elastin-derived peptide gvgvagvg," *Biomacromolecules*, vol. 12, no. 5, pp. 1546–1555, 2011.

[11] D. Pinotsi, A. K. Buell, C. M. Dobson, G. S. Kaminski Schierle, and C. F. Kaminski, "A label-free, quantitative assay of amyloid fibril growth based on intrinsic fluorescence," *ChemBioChem*, vol. 14, no. 7, pp. 846–850, 2013.

[12] J. S. Lee, E. Um, J.-K. Park, and C. B. Park, "Microfluidic self-assembly of insulin monomers into amyloid fibrils on a solid surface," *Langmuir*, vol. 24, no. 14, pp. 7068–7071, 2008.

[13] J. S. Lee, J. Ryu, and C. B. Park, "High-throughput analysis of alzheimer's β-amyloid aggregation using a microfluidic self-assembly of monomersf," *Analytical chemistry*, vol. 81, no. 7, pp. 2751–2759, 2009.

[14] J. S. Lee and C. B. Park, "Microfluidic dissociation and clearance of alzheimer's β-amyloid aggregates," *Biomaterials*, vol. 31, no. 26, pp. 6789–6795, 2010.

[15] K. Islam, Y.-C. Jang, R. Chand, S. K. Jha, H. H. Lee, and Y.-S. Kim, "Microfluidic biosensor for β-amyloid (1-42) detection using cyclic voltammetry," *Journal of nanoscience and nanotechnology*, vol. 11, no. 7, pp. 5657–5662, 2011.

[16] T. P. Knowles, D. A. White, A. R. Abate, J. J. Agresti, S. I. Cohen, R. A. Sperling, E. J. De Genst, C. M. Dobson, and D. A. Weitz, "Observation of spatial propagation of amyloid assembly from single nuclei," *Proceedings of the National Academy of Sciences*, vol. 108, no. 36, pp. 14746–14751, 2011.

[17] V. Foderá, S. Pagliara, O. Otto, U. F. Keyser, and A. M. Donald, "Microfluidics reveals a flow-induced large-scale polymorphism of protein aggregates," *The Journal of Physical Chemistry Letters*, vol. 3, no. 19, pp. 2803–2807, 2012.

[18] P. S. Dittrich and A. Manz, "Lab-on-a-chip: microfluidics in drug discovery," *Nature Reviews Drug Discovery*, vol. 5, no. 3, pp. 210–218, 2006.

[19] R. N. Zare and S. Kim, "Microfluidic platforms for single-cell analysis," *Annual review of biomedical engineering*, vol. 12, pp. 187–201, 2010.

[20] W. P. Esler, E. R. Stimson, J. M. Jennings, H. V. Vinters, J. R. Ghilardi, J. P. Lee, P. W. Mantyh, and J. E. Maggio, "Alzheimer's disease amyloid propagation by a template-dependent dock-lock mechanism," *Biochemistry*, vol. 39, no. 21, pp. 6288–6295, 2000.

[21] Y. A. Domanov and P. K. Kinnunen, "Antimicrobial peptides temporins b and l induce formation of tubular lipid protrusions from supported phospholipid bilayers," *Biophysical journal*, vol. 91, no. 12, pp. 4427–4439, 2006.

[22] Y. A. Domanov and P. K. Kinnunen, "Islet amyloid polypeptide forms rigid lipid–protein amyloid fibrils on supported phospholipid bilayers," *Journal of molecular biology*, vol. 376, no. 1, pp. 42–54, 2008.

[23] M. R. Nilsson, "Techniques to study amyloid fibril formation in vitro," *Methods*, vol. 34, no. 1, pp. 151–160, 2004.

[24] T. R. Jahn and S. E. Radford, "The yin and yang of protein folding," *FEBS Journal*, vol. 272, no. 23, pp. 5962–5970, 2005.

[25] T. R. Jahn and S. E. Radford, "Folding versus aggregation: polypeptide conformations on competing pathways," *Archives of biochemistry and biophysics*, vol. 469, no. 1, pp. 100–117, 2008.

[26] R. Wetzel, "Kinetics and thermodynamics of amyloid fibril assembly," *Accounts of chemical research*, vol. 39, no. 9, pp. 671–679, 2006.

[27] E. Eanes and G. Glenner, "X-ray diffraction studies on amyloid filaments," *Journal of Histochemistry & Cytochemistry*, vol. 16, no. 11, pp. 673–677, 1968.

[28] J. L. Jimenez, J. I. Guijarro, E. Orlova, J. Zurdo, C. M. Dobson, M. Sunde, and H. R. Saibil, "Cryo-electron microscopy structure of an sh3 amyloid fibril and model of the molecular packing," *The EMBO journal*, vol. 18, no. 4, pp. 815–821, 1999.

[29] C. Goldsbury, J. Kistler, U. Aebi, T. Arvinte, and G. J. Cooper, "Watching amyloid fibrils grow by time-lapse atomic force microscopy," *Journal of molecular biology*, vol. 285, no. 1, pp. 33–39, 1999.

[30] J. Gillam and C. MacPhee, "Modelling amyloid fibril formation kinetics: mechanisms of nucleation and growth," *Journal of Physics: Condensed Matter*, vol. 25, no. 37, p. 373101, 2013.

[31] P. Arosio, T. P. Knowles, and S. Linse, "On the lag phase in amyloid fibril formation," *Physical Chemistry Chemical Physics*, vol. 17, no. 12, pp. 7606–7618, 2015.

[32] J. D. Harper and P. T. Lansbury Jr, "Models of amyloid seeding in alzheimer's disease and scrapie: mechanistic truths and physiological consequences of the time-dependent solubility of amyloid proteins," *Annual review of biochemistry*, vol. 66, no. 1, pp. 385–407, 1997.

[33] R. Sabaté, M. Gallardo, and J. Estelrich, "Temperature dependence of the nucleation constant rate in β amyloid fibrillogenesis," *International journal of biological macromolecules*, vol. 35, no. 1, pp. 9–13, 2005.

[34] B. Morel, L. Varela, A. I. Azuaga, and F. Conejero-Lara, "Environmental conditions affect the kinetics of nucleation of amyloid fibrils and determine their morphology," *Biophysical journal*, vol. 99, no. 11, pp. 3801–3810, 2010.

[35] K. Brejc, T. K. Sixma, P. A. Kitts, S. R. Kain, R. Y. Tsien, M. Ormö, and S. J. Remington, "Structural basis for dual excitation and photoisomerization of the aequorea victoria green fluorescent protein," *Proceedings of the National Academy of Sciences*, vol. 94, no. 6, pp. 2306–2311, 1997.

[36] O. G. Mouritsen, *Life-as a matter of fat: the emerging science of lipidomics*. Springer Science & Business Media, 2005.

[37] *AOCS Lipid Library*. Available at http://lipidlibrary.aocs.org/Biochemistry/content.cfm?ItemNumber=39191. April 2016.

[38] J. H. Fendler, *The colloidal domain: Where physics, chemistry, biology, and technology meet. By D. Fennell Evans and Hakån Wennerström. VCH Publishers, New York 1994, XXXII, 515 pp., ISBN 1–56081–525–6*. Wiley Online Library, 1996.

[39] J. N. Israelachvili, D. J. Mitchell, and B. W. Ninham, "Theory of self-assembly of hydrocarbon amphiphiles into micelles and bilayers," *Journal of the Chemical Society, Faraday Transactions 2: Molecular and Chemical Physics*, vol. 72, pp. 1525–1568, 1976.

[40] G. Van Meer, D. R. Voelker, and G. W. Feigenson, "Membrane lipids: where they are and how they behave," *Nature reviews molecular cell biology*, vol. 9, no. 2, pp. 112–124, 2008.

[41] J. H. Ipsen and O. G. Mouritsen, "Modelling the phase equilibria in two-component membranes of phospholipids with different acyl-chain lengths," *Biochimica et Biophysica Acta (BBA)-Biomembranes*, vol. 944, no. 2, pp. 121–134, 1988.

[42] O. G. Mouritsen and K. Jørgensen, "Dynamical order and disorder in lipid bilayers," *Chemistry and physics of lipids*, vol. 73, no. 1, pp. 3–25, 1994.

[43] N. Craig, R. Green, C. Greider, O. Cohen-Fix, G. Storz, and C. Wolberger, *Molecular biology: principles of genome function*. OUP Oxford, 2014.

[44] E. T. Castellana and P. S. Cremer, "Solid supported lipid bilayers: From biophysical studies to sensor design," *Surface Science Reports*, vol. 61, no. 10, pp. 429–444, 2006.

[45] M. Ø. Jensen and O. G. Mouritsen, "Lipids do influence protein function—the hydrophobic matching hypothesis revisited," *Biochimica et Biophysica Acta (BBA)-Biomembranes*, vol. 1666, no. 1, pp. 205–226, 2004.

[46] R. Sood, Y. Domanov, and P. K. Kinnunen, "Fluorescent temporin b derivative and its binding to liposomes," *Journal of fluorescence*, vol. 17, no. 2, pp. 223–234, 2007.

[47] D. Thirumalai, D. Klimov, and R. Dima, "Emerging ideas on the molecular basis of protein and peptide aggregation," *Current opinion in structural biology*, vol. 13, no. 2, pp. 146–159, 2003.

[48] M. Stefani, "Protein misfolding and aggregation: new examples in medicine and biology of the dark side of the protein world," *Biochimica et Biophysica Acta (BBA)-Molecular Basis of Disease*, vol. 1739, no. 1, pp. 5–25, 2004.

[49] E. Sparr, M. F. Engel, D. V. Sakharov, M. Sprong, J. Jacobs, B. de Kruijff, J. W. Höppener, and J. A. Killian, "Islet amyloid polypeptide-induced

membrane leakage involves uptake of lipids by forming amyloid fibers," *FEBS letters*, vol. 577, no. 1, pp. 117–120, 2004.

[50] H. Zhao, E. K. Tuominen, and P. K. Kinnunen, "Formation of amyloid fibers triggered by phosphatidylserine-containing membranes," *Biochemistry*, vol. 43, no. 32, pp. 10302–10307, 2004.

[51] J.-X. Lu, K. Damodaran, J. Blazyk, and G. A. Lorigan, "Solid-state nuclear magnetic resonance relaxation studies of the interaction mechanism of antimicrobial peptides with phospholipid bilayer membranes," *Biochemistry*, vol. 44, no. 30, pp. 10208–10217, 2005.

[52] J. Blazyk, R. Wiegand, J. Klein, J. Hammer, R. M. Epand, R. F. Epand, W. L. Maloy, and U. P. Kari, "A novel linear amphipathic β-sheet cationic antimicrobial peptide with enhanced selectivity for bacterial lipids," *Journal of Biological Chemistry*, vol. 276, no. 30, pp. 27899–27906, 2001.

[53] J.-x. Lu, J. Blazyk, and G. A. Lorigan, "Exploring membrane selectivity of the antimicrobial peptide kigaki using solid-state nmr spectroscopy," *Biochimica et Biophysica Acta (BBA)-Biomembranes*, vol. 1758, no. 9, pp. 1303–1313, 2006.

[54] H. Zhao, A. Jutila, T. Nurminen, S. A. Wickström, J. Keski-Oja, and P. K. Kinnunen, "Binding of endostatin to phosphatidylserine-containing membranes and formation of amyloid-like fibers," *Biochemistry*, vol. 44, no. 8, pp. 2857–2863, 2005.

[55] R. L. Joseph and R. Lakowicz, *Principles of fluorescence spectroscopy*. Kluwer Academic/Plenum Publishers, New York, 1999.

[56] G. Bains, A. B. Patel, and V. Narayanaswami, "Pyrene: a probe to study protein conformation and conformational changes," *Molecules*, vol. 16, no. 9, pp. 7909–7935, 2011.

[57] P. Somerharju, "Pyrene-labeled lipids as tools in membrane biophysics and cell biology," *Chemistry and physics of lipids*, vol. 116, no. 1, pp. 57–74, 2002.

[58] B. Valeur and M. N. Berberan-Santos, *Molecular fluorescence: principles and applications*. John Wiley & Sons, 2012.

[59] A. Ulman, "Formation and structure of self-assembled monolayers," *Chemical reviews*, vol. 96, no. 4, pp. 1533–1554, 1996.

[60] R. G. Nuzzo and D. L. Allara, "Adsorption of bifunctional organic disulfides on gold surfaces," *Journal of the American Chemical Society*, vol. 105, no. 13, pp. 4481–4483, 1983.

[61] J. P. Folkers, P. E. Laibinis, and G. M. Whitesides, "Self-assembled monolayers of alkanethiols on gold: comparisons of monolayers containing mixtures of short-and long-chain constituents with methyl and hydroxymethyl terminal groups," *Langmuir*, vol. 8, no. 5, pp. 1330–1341, 1992.

[62] S. Thomas, S. Rafiei, S. Maghsoodlou, and A. Afzali, *Foundations of Nanotechnology, Volume Two: Nanoelements Formation and Interaction*. CRC Press, 2014.

[63] L. H. Dubois and R. G. Nuzzo, "Synthesis, structure, and properties of model organic surfaces," *Annual review of physical chemistry*, vol. 43, no. 1, pp. 437–463, 1992.

[64] e. a. Porter, Marc D., "Spontaneously organized molecular assemblies. 4. structural characterization of n-alkyl thiol monolayers on gold by optical ellipsometry, infrared spectroscopy, and electrochemistry," *Journal of the American Chemical Society*, vol. 109, no. 12, pp. 3559–3568, 1987.

[65] B. M. Lamb, D. G. Barrett, N. P. Westcott, and M. N. Yousaf, "Microfluidic lithography of sams on gold to create dynamic surfaces for directed cell migration and contiguous cell cocultures," *Langmuir*, vol. 24, no. 16, pp. 8885–8889, 2008.

[66] E. K. Sackmann, A. L. Fulton, and D. J. Beebe, "The present and future role of microfluidics in biomedical research," *Nature*, vol. 507, no. 7491, pp. 181–189, 2014.

[67] A. J. Demello, "Control and detection of chemical reactions in microfluidic systems.," *Nature*, vol. 442, no. 7101, pp. 394–402, 2006.

[68] Y. Liao and Y. Cheng, "Femtosecond laser 3d fabrication in porous glass for micro-and nanofluidic applications," *Micromachines*, vol. 5, no. 4, pp. 1106–1134, 2014.

[69] C.-Y. Lee, C.-L. Chang, Y.-N. Wang, and L.-M. Fu, "Microfluidic mixing: a review," *International journal of molecular sciences*, vol. 12, no. 5, pp. 3263–3287, 2011.

[70] T. M. Squires and S. R. Quake, "Microfluidics: Fluid physics at the nanoliter scale," *Reviews of modern physics*, vol. 77, no. 3, p. 977, 2005.

[71] S. C. Terry, J. H. Jerman, and J. B. Angell, "A gas chromatographic air analyzer fabricated on a silicon wafer," *Electron Devices, IEEE Transactions on*, vol. 26, no. 12, pp. 1880–1886, 1979.

[72] G. T. Roman, T. Hlaus, K. J. Bass, T. G. Seelhammer, and C. T. Culbertson, "Sol-gel modified poly (dimethylsiloxane) microfluidic devices with high electroosmotic mobilities and hydrophilic channel wall characteristics," *Analytical chemistry*, vol. 77, no. 5, pp. 1414–1422, 2005.

[73] F. K. Balagaddé, L. You, C. L. Hansen, F. H. Arnold, and S. R. Quake, "Long-term monitoring of bacteria undergoing programmed population control in a microchemostat," *Science*, vol. 309, no. 5731, pp. 137–140, 2005.

[74] M. Focke, F. Stumpf, B. Faltin, P. Reith, D. Bamarni, S. Wadle, C. Müller, H. Reinecke, J. Schrenzel, P. Francois, *et al.*, "Microstructuring of polymer

films for sensitive genotyping by real-time pcr on a centrifugal microfluidic platform," *Lab on a Chip*, vol. 10, no. 19, pp. 2519–2526, 2010.

[75] M. J. Jebrail, M. S. Bartsch, and K. D. Patel, "Digital microfluidics: a versatile tool for applications in chemistry, biology and medicine," *Lab on a Chip*, vol. 12, no. 14, pp. 2452–2463, 2012.

[76] X. Li, D. R. Ballerini, and W. Shen, "A perspective on paper-based microfluidics: current status and future trends," *Biomicrofluidics*, vol. 6, no. 1, p. 011301, 2012.

[77] A. R. Prakash, S. Adamia, V. Sieben, P. Pilarski, L. Pilarski, and C. Backhouse, "Small volume pcr in pdms biochips with integrated fluid control and vapour barrier," *Sensors and Actuators B: Chemical*, vol. 113, no. 1, pp. 398–409, 2006.

[78] M. A. Unger, H.-P. Chou, T. Thorsen, A. Scherer, and S. R. Quake, "Monolithic microfabricated valves and pumps by multilayer soft lithography," *Science*, vol. 288, no. 5463, pp. 113–116, 2000.

[79] T. Merkel, V. Bondar, K. Nagai, B. Freeman, and I. Pinnau, "Gas sorption, diffusion, and permeation in poly (dimethylsiloxane)," *Journal of Polymer Science Part B: Polymer Physics*, vol. 38, no. 3, pp. 415–434, 2000.

[80] S. Worden, R. Morad, *Quartz Cementation in Sandstones.* John Wiley & Sons, 2009.

[81] R. P. Richter, R. Bérat, and A. R. Brisson, "Formation of solid-supported lipid bilayers: an integrated view," *Langmuir*, vol. 22, no. 8, pp. 3497–3505, 2006.

[82] P. Kim, S. E. Lee, H. S. Jung, H. Y. Lee, T. Kawai, and K. Y. Suh, "Soft lithographic patterning of supported lipid bilayers onto a surface and inside microfluidic channels," *Lab on a Chip*, vol. 6, no. 1, pp. 54–59, 2006.

[83] P. Jonsson, J. P. Beech, J. O. Tegenfeldt, and F. Hook, "Shear-driven motion of supported lipid bilayers in microfluidic channels," *Journal of the American Chemical Society*, vol. 131, no. 14, pp. 5294–5297, 2009.

[84] T. Gervais, J. El-Ali, A. Günther, and K. F. Jensen, "Flow-induced deformation of shallow microfluidic channels," *Lab on a Chip*, vol. 6, no. 4, pp. 500–507, 2006.

[85] T. Lührs, C. Ritter, M. Adrian, D. Riek-Loher, B. Bohrmann, H. Döbeli, D. Schubert, and R. Riek, "3d structure of alzheimer's amyloid-β (1–42) fibrils," *Proceedings of the National Academy of Sciences of the United States of America*, vol. 102, no. 48, pp. 17342–17347, 2005.

[86] P. Wadhwani, E. Strandberg, N. Heidenreich, J. Buürck, S. Fanghänel, and A. S. Ulrich, "Self-assembly of flexible β-strands into immobile amyloid-like β-sheets in membranes as revealed by solid-state 19f nmr," *Journal of the American Chemical Society*, vol. 134, no. 15, pp. 6512–6515, 2012.

[87] P. Wadhwani, J. Reichert, E. Strandberg, J. Bürck, J. Misiewicz, S. Afonin, N. Heidenreich, S. Fanghänel, P. K. Mykhailiuk, I. V. Komarov, *et al.*, "Stereochemical effects on the aggregation and biological properties of the fibril-forming peptide [kigaki] 3 in membranes," *Physical Chemistry Chemical Physics*, vol. 15, no. 23, pp. 8962–8971, 2013.

[88] J. Lai, C. Zheng, D. Liang, and Y. Huang, "Amyloid-like fibrils formed by ε-poly-l-lysine," *Biomacromolecules*, vol. 14, no. 12, pp. 4515–4519, 2013.

[89] V. Torchilin and V. Weissig, *Liposomes: a practical approach*. No. 264, Oxford University Press, 2003.

[90] R. Tejera-Garcia, S. Ranjan, V. Zamotin, R. Sood, and P. K. Kinnunen, "Making unilamellar liposomes using focused ultrasound," *Langmuir*, vol. 27, no. 16, pp. 10088–10097, 2011.

[91] J. Reichman, "Handbook of optical filters for fluorescence microscopy," *Chroma Technology Corporation*, 2000.

[92] Zeiss, "Education in microscopy and digital imaging." URL: http://zeiss-campus.magnet.fsu.edu/articles/lightsources/mercuryarc.html, Retrieved 4 May 2016.

[93] E. Barsoukov and J. R. Macdonald, *Impedance spectroscopy: theory, experiment, and applications*. John Wiley & Sons, 2005.

[94] P. K. Kinnunen, K. Kaarniranta, and A. K. Mahalka, "Protein-oxidized phospholipid interactions in cellular signaling for cell death: From biophysics to clinical correlations," *Biochimica et Biophysica Acta (BBA)-Biomembranes*, vol. 1818, no. 10, pp. 2446–2455, 2012.

[95] D. M. Byler and H. Susi, "Examination of the secondary structure of proteins by deconvolved ftir spectra," *Biopolymers*, vol. 25, no. 3, pp. 469–487, 1986.

[96] M. Breton, M. Amirkavei, and L. M. Mir, "Optimization of the electroformation of giant unilamellar vesicles (guvs) with unsaturated phospholipids," *The Journal of membrane biology*, vol. 248, no. 5, pp. 827–835, 2015.

[97] M. Heim, G. Cevc, R. Guckenberger, H. F. Knapp, and W. Wiegräbe, "Lateral electrical conductivity of mica-supported lipid bilayer membranes measured by scanning tunneling microscopy.," *Biophysical journal*, vol. 69, no. 2, p. 489, 1995.

[98] P. K. Kinnunen and J. A. Virtanen, "A qualitative, molecular model of the nerve impulse," in *Modern Bioelectrochemistry*, pp. 457–479, Springer, 1986.

[99] R. F. De Almeida, A. Fedorov, and M. Prieto, "Sphingomyelin/phosphatidylcholine/cholesterol phase diagram: boundaries and composition of lipid rafts," *Biophysical journal*, vol. 85, no. 4, pp. 2406–2416, 2003.

[100] S.-J. Ding, B.-W. Chang, C.-C. Wu, M.-F. Lai, and H.-C. Chang, "Impedance spectral studies of self-assembly of alkanethiols with different chain lengths using different immobilization strategies on au electrodes," *Analytica Chimica Acta*, vol. 554, no. 1, pp. 43–51, 2005.

A Impedance Measurements with Buffer

Impedance measurements with POPC:PPDG, PPDPC:PPDPG, and DMPC:DMPG SLBs in 20 mM HEPES, 0.1 mM EDTA buffer (pH 7). The buffer seemed to have a considerable effect to the measurements.

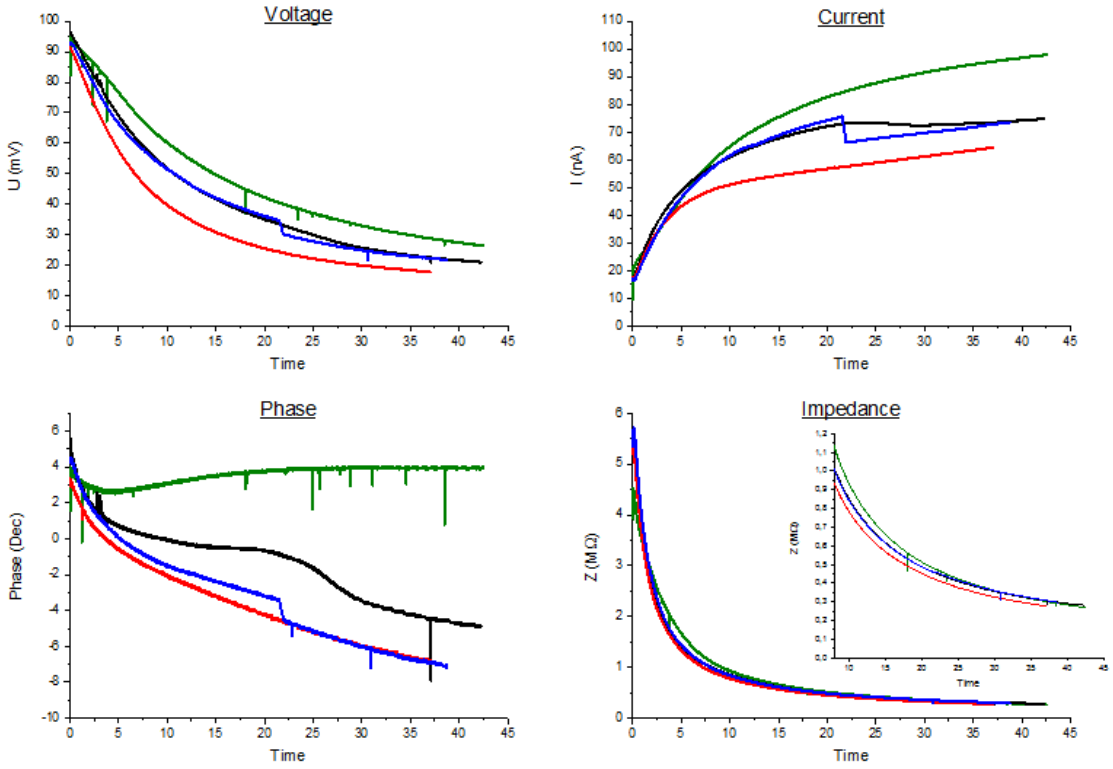

Figure A1: Conductivity data during incubation of 20 mM HEPES, 0.1 mM EDTA buffer (—), POPC:PPDPG (—), PPDPC:PPDPG (—), and DMPC:DMPG (—) SLBs in buffer. PC:PG (mol%:mol%) relation was 80:20 in each SLB.

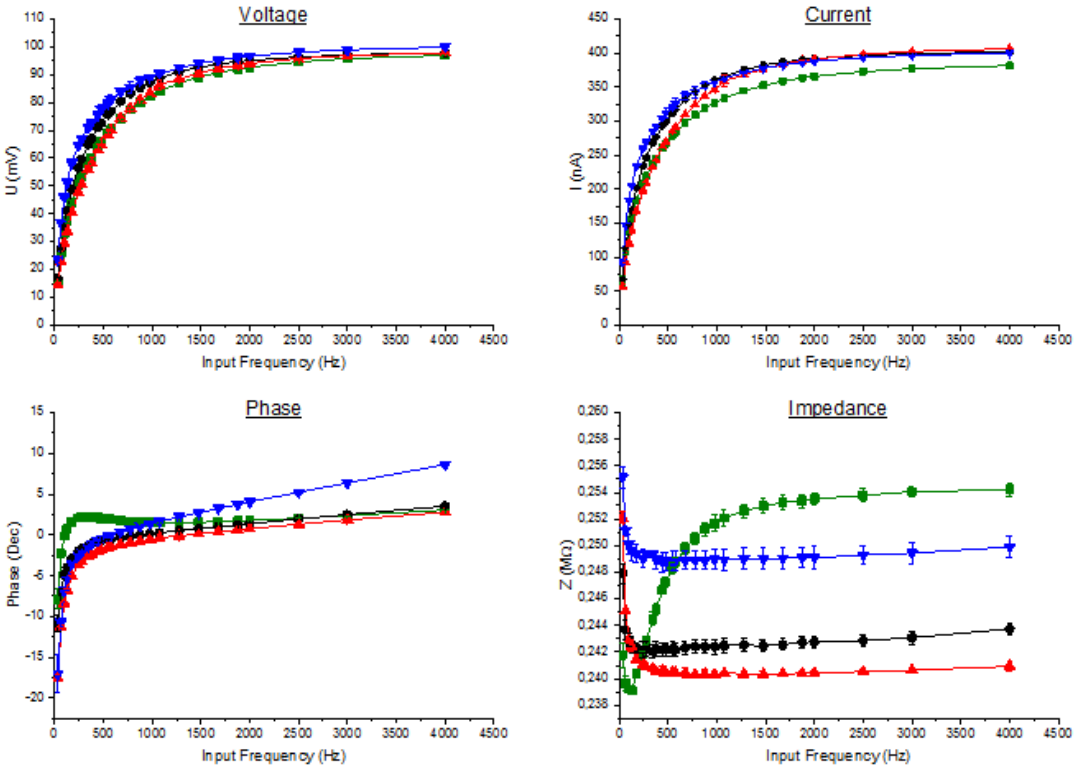

Figure A2: Frequency characteristics of 20 mM HEPES, 0.1 mM EDTA buffer (■), POPC:PPDPG (●), PPDPC:PPDPG (▲), and DMPC:DMPG (▼) SLBs in buffer. 0.4 V is used as input voltage. PC:PG (mol%:mol%) relation was 80:20 in each SLB.

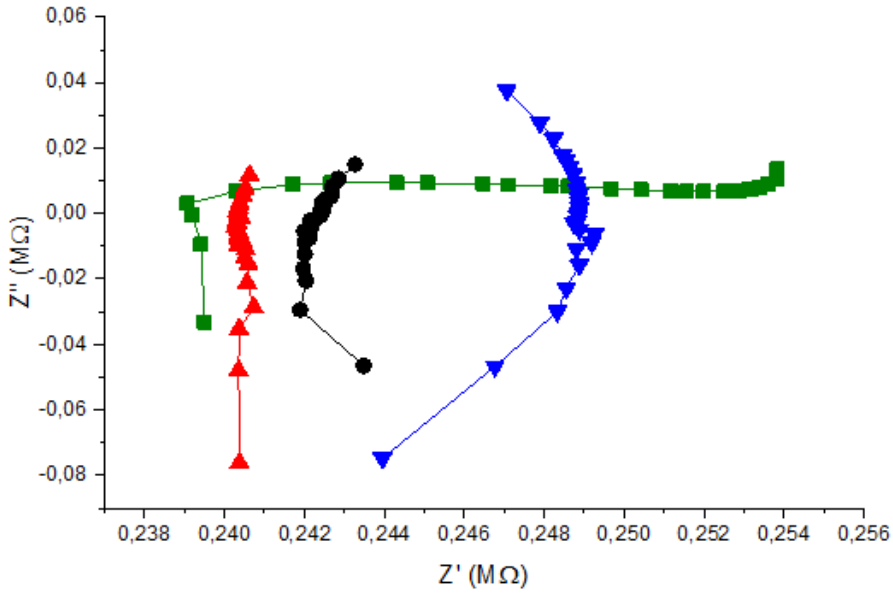

Figure A3: Impedance of 20 mM HEPES, 0.1 mM EDTA buffer (■), POPC:PPDPG (●), (▲), and DMPC:DMPG (▼) SLBs in buffer in Cartesian coordinates. PC:PG (mol%:mol%) relation was 80:20 in each SLB.

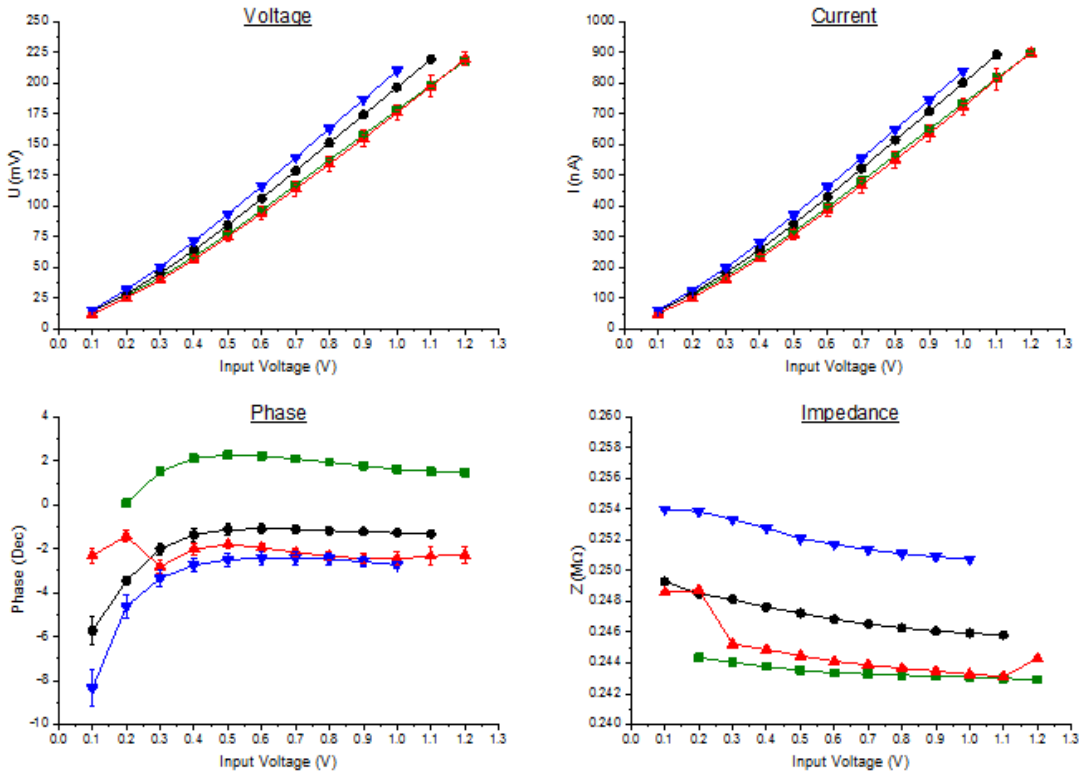

Figure A4: Voltage characteristics of 20 mM HEPES, 0.1 mM EDTA buffer (■), POPC:PPDPG (●), PPDPC:PPDPG)(▲), and DMPC:DMPG(▼) SLBs in buffer. 344 Hz is used as input frequency. PC:PG (mol%:mol%) relation was 80:20 in each SLB.